THE JOURNAL OF PHYSICAL CHEMISTRY A

Article

pubs.acs.org/JPCA

Disproportionation of Bromous Acid HOBrO by Direct O-Transfer and via Anhydrides $O(BrO)_2$ and $BrO-BrO_2$. An Ab Initio Study of the Mechanism of a Key Step of the Belousov–Zhabotinsky Oscillating Reaction

Rainer Glaser*,† and Mary Jost†

†Department of Chemistry, University of Missouri, Columbia, Missouri 65211, United States

Supporting Information

ABSTRACT: The results are reported of an ab initio study of the thermochemistry and of the kinetics of the HOBrO disproportionation reaction 2HOBrO (**2**) ⇄ HOBr (**1**) + $HBrO_3$ (**3**), reaction (R4′), in gas phase (MP2(full)/6-311G*) and aqueous solution (SMD(MP2(full)/6-311G*)). The reaction energy of bromous acid disproportionation is discussed in the context of the coupled reaction system R2–R4 of the FKN mechanism of the Belousov–Zhabotinsky reaction and considering the acidities of HBr and $HOBrO_2$. The structures were determined of ten dimeric aggregates **4** of bromous acid, $(HOBrO)_2$, of eight mixed aggregates **5** formed between the products of disproportionation, $(HOBr)(HOBrO_2)$, and of four transition states structures **6** for disproportionation by direct O-transfer. It was found that the condensation of two HOBrO molecules provides facile access to bromous acid anhydride **7**, $O(BrO)_2$. A discussion of the potential energy surface of Br_2O_3 shows that $O(BrO)_2$ is prone to isomerization to the mixed anhydride **8**, $BrO-BrO_2$, and to dissociation to **9**, BrO, and **10**, BrO_2, and their radical pair **11**. Hence, three possible paths from $O(BrO)_2$ to the products of disproportionation, HOBr and $HOBrO_2$, are discussed: (1) hydrolysis of $O(BrO)_2$ along a path that differs from its formation, (2) isomerization of $O(BrO)_2$ to $BrO-BrO_2$ followed by hydrolysis, and (3) $O(BrO)_2$ dissociation to BrO and BrO_2 and their reactions with water. The results of the potential energy surface analysis show that the rate-limiting step in the disproportionation of HOBrO consists of the formation of the hydrate **12a** of bromous acid anhydride **7** via transition state structure **14a**. The computed activation free enthalpy ΔG_{act}(SMD) = 13.6 kcal/mol for the process 2·**2a** → [**14a**]‡ → **12a** corresponds to the reaction rate constant k_4 = 667.5 M^{-1} s^{-1} and is in very good agreement with experimental measurements. The potential energy surface analysis further shows that anhydride **7** is kinetically and thermodynamically unstable with regard to hydrolysis to HOBr and $HOBrO_2$ via transition state structure **14b**. The transition state structure **14b** is much more stable than **14a**, and, hence, the formation of the "symmetrical anhydride" from bromous acid becomes an irreversible reaction for all practical purposes because **7** will instead be hydrolyzed as a "mixed anhydride" to afford HOBr and $HOBrO_2$. The mixed anhydride **8**, $BrO-BrO_2$, does not play a significant role in bromous acid disproportionation.

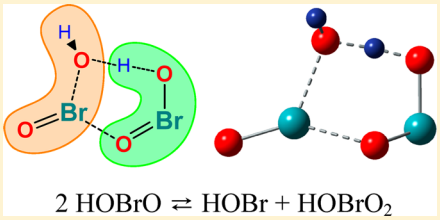

INTRODUCTION

The first oscillating reaction was reported by Belousov in 1958,[1] and it consisted of the cerium-catalyzed bromate oxidation of citric acid, $HOOC-C(OH)(CH_2COOH)_2$, in aqueous sulfuric acid solution. Zhabotinsky also employed malic acid, $HOOC-CH(OH)-CH_2COOH$, and malonic acid, $H_2C(COOH)_2$, in his seminal 1970 paper.[2] Today, the cerium-catalyzed bromate oxidation of malonic acid in aqueous sulfuric acid solution is considered as the classic Belousov–Zhabotinsky reaction (BZR).[3,4] The color of the reaction solution of the classic BZR oscillates between yellow and colorless reflecting the oscillations between Ce(IV) and Ce(III) species, respectively. A frequently studied variation of the BZR employs iron salts in the presence of phenanthroline and this ferroin-BZR[5,6] displays impressive oscillations between red ferroin $[Fe(phen)_3]^{2+}$ and blue ferrin $[Fe(phen)_3]^{3+}$, and other metals also have been studied (Ru,[7] Mn[8]). Since the pioneering discoveries of Belousov and Zhabotinsky, a number of other oscillating chemical reactions as well as biological reactions have been discovered and studied, but the significance of the BZR as the mainstay reaction of nonlinear chemical dynamics remains unrivaled.[9] Current interests in the BZ reaction are concerned with detailed analyses of the organic products including CO and CO_2 formations,[10,11] de novo designs of new oscillating systems,[12] the study of light-emitting oscillating reactions,[13] and most recently the analysis of microemulsions[14] and polymer-gels.[15]

$$H^+ + Br^- + HOBrO \rightleftarrows 2HOBr \quad (R2)$$

$$2H^+ + Br^- + BrO_3^- \rightleftarrows HOBr + HOBrO \quad (R3)$$

$$2HOBrO \rightleftarrows HOBr + H^+ + BrO_3^- \quad (R4)$$

Received: February 9, 2012
Revised: July 17, 2012

   dx.doi.org/10.1021/jp301329g | J. Phys. Chem. A XXXX, XXX, XXX–XXX

Table 1. Reported Kinetic Parameters of the Disproportionation of Bromous Acid

year	authors	medium	k_4 (M^{-1} s^{-1}))	k_{-4} (M^{-2} s^{-1})	activation parameters[c]
1972	Field, Körös, and Noyes	≈1 M H_2SO_4	4×10^7	2×10^{-10}	
1979	Sullivan and Thompson	1.5 M H_2SO_4	$<6 \times 10^3$		
1983	Noszticzius,	0.15 M H_2SO_4	$1.4 \pm 0.2 \times 10^3$		
	Noszticzius and Schelly	1.5 M H_2SO_4	$3.8 \pm 1 \times 10^3$		
1983	Försterling et al.		4×10^8		
1986	Ariese and Nagy-Ungvarai	0.5 M H_2SO_4	2.2×10^3		
1986	Field and Försterling	≈1 M H_2SO_4	3000	1×10^{-8}	
1993	Försterling and Varga	2 M H_2SO_4	8000		
1994	Faria, Epstein, Kustin	pH 3.9−5.6[a]	≈800 ± 100		
1994	Faria, Epstein, Kustin	pH 5.9−8.0[b]	≈39.1 ± 2.6		
2006	Agreda and Field	30−90 mM H_2SO_4	≈1700		$\Delta E^{\ddagger} = 5.5 \pm 0.1$
					$\Delta S^{\ddagger} = -28.4 \pm 0.2$
2006	Agreda and Field	4−9 mM $HClO_4$	781 ± 6		$\Delta E^{\ddagger} = 4.5 \pm 0.2$
					$\Delta S^{\ddagger} = -31.5 \pm 0.7$

[a]Acetate buffer. [b]Phosphate buffer. [c]$\Delta E^{\ddagger}$ in kcal/mol and $\Delta S^{\ddagger}$ in cal/(K mol).

In 1972, Field, Körös, and Noyes published two seminal papers on the mechanism of the BZ reaction, and their model included ten reactions. The first seven reactions together with the respective reaction rate constants are now widely referred to as the FKN model.[16] The disproportionation of bromous acid plays a prominent role as "Reaction 4″ (or R4 for short) in the FKN model. Alternative models have been discussed,[17] and these include in particular the Györgyi-Field (GF) model of eight reactions proposed in 1991[18] and the Marburg-Budapest-Missoula (MBM) model proposed in 2001.[19] It is a key feature of the GF model that HOBr does not appear in the reactions. Reaction GF3 takes the place of R4 in that bromous acid reacts with itself in a bimolecular, irreversible reaction ($r_{GF3} = k_{GF3}$ [HOBrO]^2) and then with malonic acid (MA) to yield bromic acid, brominated malonic acid ($BrCH(COOH)_2$, BrMA) and water. Reaction GF3 can formally be understood as the combination of R4 with the faster reaction HOBr + MA → BrMA + H_2O, but the GF mechanism allows for the possibility of BrO_x radicals reacting directly with MA. It is an important feature of the MBM model that the neutral disproportionation FKN-R4 is replaced by the protonation of bromous acid HOBrO + H^+ → $H_2BrO_2^+$ (MBM-R4)[20] and the proton-catalyzed reaction HOBrO + $H_2BrO_2^+$ → HOBr + BrO_3^- + $2H^+$ (MBM-R5).

The reaction rate constants $k_4 = 4 \times 10^{+7}$ M^{-1} s^{-1} and $k_{-4} = 2 \times 10^{-10}$ M^{-2} s^{-1}, respectively, for the forward and backward reactions, respectively, show the disproportionation of bromous acid to be very fast and irreversible (Table 1). The equilibrium constant $K_4 = k_4/k_{-4} = 2 \times 10^{+17}$ M corresponds to a reaction free enthalpy $\Delta G_4 = -23.6$ kcal/mol. A few years later Försterling et al.[21] published an even higher k_4 value. Yet, Sullivan and Thompson[22] observed the kinetics of the Ce(IV)-bromous acid reaction in 1.5 M H_2SO_4 by stopped-flow methods and concluded in 1979 that the FKN estimate of k_4 must be much too large, and their work suggested $k_4 < 6 \times 10^{+3}$ M^{-1} s^{-1}. The bromous acid disproportionation is a key step of the BZ reaction, and several studies in the following two decades were aimed at clarifying the reaction kinetics. In 1983, Noszticzius, Noszticzius, and Schelly monitored the disproportionation reaction of (bromide-free) bromous acid with ion-selective electrodes in 0.15 and 1.5 M H_2SO_4.[23] The acidity of the medium affects the measured k_4 values (Table 1), but both measured k_4 values where several magnitudes lower than the FNK value. In 1986, Ariese and Nagy-Ungvarai[24] measured the bromous acid disproportionation reaction using stopped-flow techniques in 0.5 M H_2SO_4 and reported $k_4 = 2.2 \times 10^{+3}$ M^{-1} s^{-1} in support of the value $k_4 = 2 \times 10^{+3}$ M^{-1} s^{-1} they attributed to Noszticzius et al.[23] for the 0.5 M H_2SO_4 medium. Also in 1986, Field and Försterling (FF) suggested an alternative set of rate constants for the BZ reaction.[25] One of the key differences between the FKN and FF parameter sets concerned the much lower forward reaction rate constant $k_4 = 3000$ M^{-1} s^{-1} of "Reaction 4" as well as the higher reaction rate constant $k_{-4} = 1 \times 10^{-8}$ M^{-2} s^{-1}. These data give an equilibrium constant $K_4 = k_4/k_{-4} = 3 \times 10^{+11}$ M corresponding to $\Delta G_4 = -15.6_6$ kcal/mol. The rate of reaction R4 increases with the acid concentration (cf. values measured in 0.5 M, 1 M, and 2 M H_2SO_4),[26] and efforts were made to measure R4 in less acidic media. In 1994, Faria, Epstein, and Kustin[27] measured the kinetics of the disproportionation reaction in phosphate buffer ($5.9 \le$ pH ≤ 8.0) and acetate buffer ($3.9 \le$ pH ≤ 5.6) by monitoring optical absorbance at 294 nm using stopped-flow methods and reported the rate constant $k_4 \approx 800 \pm 100$ M^{-1} s^{-1}. In 2006, Agreda and Field studied the HOBrO disproportionation in aqueous $HClO_4$ and aqueous H_2SO_4.[28] The reactions were found to be clean second-order reactions, and the experimental rate constant k_{exp} was treated as superposition of one pH-independent and one pH-dependent reaction, $k_{exp} = k + k'\cdot[H^+]$, and the data reported for the pH-independent reaction are included in Table 1. Agreda and Field derived the standard enthalpy of formation of bromous acid $\Delta^f H_0\{HBrO_2(aq)\} = -7.9$ kcal/mol and determined the reaction enthalpy of R4 to be $\Delta H_4 = -27.2_3$ kcal/mol. With the FF-value $\Delta G_4 = -15.6_6$ kcal/mol, the reaction entropy becomes $\Delta S_4 = -40.1$ cal/(K mol).[29]

In this article we report the results of an ab initio study of the thermochemistry and of the kinetics of the HOBrO disproportionation in gas phase and aqueous solution. We begin with a study of hypobromous acid **1**, bromous acid **2**, and bromic acid **3** and discuss the reaction energy of bromous acid disproportionation in the context of the coupled reaction system R2−R4 and considering the protonation states of HBr and $HOBrO_2$. Next, we report results of studies of dimeric aggregates **4** of bromous acid, $(HOBrO)_2$ and of mixed aggregates **5** formed between the products of disproportionation, $(HOBr)(HOBrO_2)$. The discussion of the aggregates guides the search for transition states structures **6** for direct O-transfer and four such transition state structures were located. The analysis of aggregates **4** and **5**, respectively, also guides the

dx.doi.org/10.1021/jp301329g | J. Phys. Chem. A XXXX, XXX, XXX−XXX

Table 2. Relative and Reaction Energies[a,b] Computed at MP2(full)/6-311G*

eq	relation/reaction	ΔE	ΔH_0	ΔH_{298}	ΔG_{298}
	E_{rel}, **1b** vs **1a**	46.28	45.28	44.93	46.36
	E_{act}, **2a** → **2b**	3.02	2.27	2.11	2.29
	E_{act}, **2a** → **2c**	8.08	7.30	7.14	7.35
	E_{act}, **3a** → **3b**	4.81	4.66	4.17	5.56
R4′	E_{rxn}, 2·**2a** → **1a** + **3a**	−30.27	−30.17	−30.01	−29.97
R2″	E_{rxn}, HBr + **2a** ⇄ 2 **1a**	−40.22	−37.91	−38.09	−39.26
R3″	E_{rxn}, HBr + **3a** ⇄ **1a** + **2a**	−9.96	−7.74	−8.08	−9.29
	E_{rel}, boat-**4a** vs chair-**4a**	2.85	2.69	2.88	2.18
	E_{dim}, 2·**2a** → chair-**4a**	−27.17	−24.84	−24.76	−12.41
	E_{rel}, **4b** vs chair-**4a**	18.03	16.46	17.44	14.40
	E_{rel}, **4c** vs chair-**4a**	18.11	16.43	17.44	14.64
	E_{rel}, cis-**4d** vs chair-**4a**	18.90	17.12	18.16	15.49
	E_{rel}, trans-**4d** vs chair-**4a**	19.01	17.25	18.31	15.39
	E_{rel}, TS(**4b**,**4c**) vs chair-**4a**	43.88	41.42	41.89	41.07
	E_{rel}, **4e** vs chair-**4a**	8.76	8.06	8.47	7.71
	E_{rel}, **4f** vs chair-**4a**	12.12	11.20	11.86	10.27
	E_{rel}, **4g** vs chair-**4a**	12.27	11.65	12.21	9.79
	E_{rel}, **4h** vs chair-**4a**	10.55	9.93	10.48	8.54
	E_{dim}, 2·**2a** → **4e**	−18.41	−16.78	−16.29	−4.70
	E_{dim}, 2·**2a** → **4f**	−15.00	−13.64	−12.89	−2.14
	E_{dim}, 2·**2a** → **4g**	−14.90	−13.18	−12.54	−2.62
	E_{dim}, 2·**2a** → **4h**	−16.61	−14.91	−14.28	−3.87
	E_{rel}, **5b** vs **5a**	1.36	1.05	1.30	−0.46
	E_{rel}, cis-**5c** vs **5a**	−7.98	−6.47	−7.34	−5.21
	E_{rel}, trans-**5c** vs **5a**	−7.43	−5.97	−6.80	−4.88
	E_{rel}, **5d** vs **5a**	−3.46	−2.67	−3.16	−2.21
	E_{rel}, cis-**5e** vs **5a**	−3.60	−3.00	−3.32	−2.57
	E_{rel}, trans-**5e** vs **5a**	−3.54	−2.93	−3.24	−2.77
	E_{rel}, **5f** vs **5a**	−2.96	−2.51	−2.69	−3.36
	E_{agg}, **1a** + **3a** → **5a**	−5.37	−4.46	−3.51	5.56
	E_{agg}, **1a** + **3a** → **5b**	−4.01	−3.42	−2.21	5.10
	E_{agg}, **1a** + **3a** → cis-**5c**	−13.35	−10.94	−10.84	0.34
	E_{agg}, **1a** + **3a** → trans-**5c**	−12.81	−10.43	−10.31	0.67
	E_{act}, **4b** → **6b**	25.85	24.96	24.44	26.67
	E_{act}, **4c** → **6c**	22.99	23.05	22.20	24.91
	E_{act}, **4e** → **6e**	33.52	33.09	32.51	33.88
	E_{act}, **4f** → **6f**	33.63	32.81	32.27	33.83
	E_{act}, 2·**2a** → **6b**	16.71	16.59	17.13	28.66
	E_{act}, 2·**2a** → **6c**	13.93	14.65	14.89	27.14
	E_{act}, 2·**2a** → **6e**	15.11	16.32	16.22	29.18
	E_{act}, 2·**2a** → **6f**	18.63	19.17	19.38	31.68
	E_{rel}, **7b** vs **7a**	1.37	1.41	1.39	1.54
	E_{act}, **7a** → **7c**	6.06	5.90	5.46	6.75
	E_{rel}, **8b** vs **8a**	0.65	0.23	−0.11	1.71
	7a → BrO + BrO_2	−0.60	−1.62	−2.32	−12.05
	BrO + BrO_2 → **8a**	−27.25	−25.37	−25.05	−15.09
	7a → **8a**	−27.85	−27.00	−27.37	−27.13

eq	relation/reaction	ΔE	ΔH_0	ΔH_{298}	ΔG_{298}
	BrO + BrO_2 → ^{3}**11b**	−4.05	−3.72	−2.61	3.41
	E_{rxn}, **4f** → **12a**	−8.88	−8.95	−8.63	−9.04
	E_{rxn}, 2·**2a** → **7a** + H_2O	−9.99	−11.27	−10.06	−9.99
	E_{rxn}, **1a** + **3a** → **7a** + H_2O	20.27	18.90	19.95	19.98
	E_{desol}, **12a** → **7a** + H_2O	13.89	11.32	11.47	1.20
	E_{act}, **4f** → **14a**	11.38	8.24	7.72	8.89
	E_{act}, 2·**2a** → **14a**	−3.62	−5.40	−5.18	6.75
	E_{act}, **12a** → **14b**	4.57	1.29	0.60	1.89
	E_{act}, **7a** + H_2O → **14b**	−9.32	−10.03	−10.87	0.69
	E_{rel}, **14a** vs **14b**	15.59	15.90	15.75	16.04
	E_{act}, **1a** + **3a** → **14b**	10.96	8.87	9.08	20.67
	E_{act}, 2·**2a** → **14c**	15.81	14.88	15.18	26.67
	E_{desol}, **12b** → **7a** + H_2O	34.18	31.91	31.90	22.11
	E_{desol}, **12b** → **8a** + H_2O	6.33	4.91	4.53	−4.91
	E_{rel}, **15e** vs **14a**	2.88	5.09	5.05	5.22
	E_{act}, 2·**2a** → **15e**	−0.74	−0.31	−0.13	11.97
	E_{desol}, **13a** → **8a** + H_2O	7.88	5.98	5.88	−4.32
	E_{desol}, **13b** → **8a** + H_2O	12.03	10.12	9.88	−0.07
	E_{desol}, **13c** → **8a** + H_2O	7.04	5.39	4.96	−3.74
	E_{desol}, **13d** → **8a** + H_2O	5.22	3.70	3.20	−5.55
	E_{rxn}, **13b** → trans-**5e**	10.77	11.07	10.64	10.42
	E_{rxn}, **13c** → trans-**5e** (via **5a**)	5.71	6.09	5.63	6.20
	E_{rxn}, **8a** + H_2O → **1a** + **3a**	7.58	8.09	7.42	7.15
	E_{rel}, **15b** vs **15a**	−1.45	0.55	0.25	1.28
	E_{rel}, **15c** vs **15a**	26.42	28.75	28.03	30.26
	E_{rel}, **15d** vs **15a**	26.93	29.07	28.37	30.59
	E_{rel}, **15e** vs **15a**	17.02	18.88	18.84	19.13
	E_{act}, **1a** + **3a** → **15a**	12.50	10.98	11.04	22.80
	E_{act}, **1a** + **3a** → **15b**	11.05	11.53	11.29	24.09
	E_{act}, **13b** → **15a**	32.11	29.19	28.34	29.88
	E_{act}, **13b** → **15b**	30.66	29.74	28.60	31.16
	E_{act}, **8a** + H_2O → **15a**	20.08	19.07	18.46	29.95
	E_{act}, **8a** + H_2O → **15b**	18.64	19.62	18.71	31.24
	E_{sol}, **8a** + 2H_2O → **16**	−27.31	−22.50	−22.62	−2.15
	E_{act}, **16** → **17**	35.55	31.86	31.47	31.21
	E_{act}, **8a** + 2H_2O → **17**	8.25	9.36	8.85	29.07
	E_{act}, **8a** + $(H_2O)_2$ → **17**	16.38	15.00	14.46	28.50
	E_{rxn}, BrO + H_2O → **1a** + HO	12.15	10.81	10.85	10.50
	E_{rxn}, BrO_2 + H_2O → **2a** + HO	39.32	38.11	38.16	38.58
	E_{rxn}, BrO + HO → **2a**	−28.72	−25.22	−25.79	−16.54
	E_{rxn}, BrO_2 + HO → **3a**	−31.82	−28.09	−28.49	−18.43
	E_{rxn}, BrO + BrO_2 + H_2O → **1a** + **3a**	−19.67	−17.28	−17.63	−7.94
	E_{act}, BrO + H_2O → **18**	23.43	21.83	21.29	29.76
	E_{act}, BrO_2 + H_2O → **19**	48.39	48.92	47.98	59.15
	E_{act}, BrO + 2H_2O → **20**	10.95	17.21	16.52	34.18
	E_{act}, BrO·H_2O + H_2O → **20**	17.73	22.91	21.70	32.59

[a]All values are in kcal/mol. [b]Two digits are provided merely for numerical accuracy.

subsequent discussions of the formations of anhydrides **7**, $O(BrO)_2$, and **8**, BrO−BrO_2, respectively. A classification of condensation reactions is described that connects two molecules of HOBrO or HOBr and $HOBrO_2$ to either **7** and **8**, and eight transition state structures of such condensation reactions have been determined. The potential energy surface analysis shows that $O(BrO)_2$ is prone to isomerization to **8** and to dissociation to **9**, BrO, and **10**, BrO_2, and their radical pair **11**. Hence, there are several options to convert $O(BrO)_2$ to the products of disproportionation, HOBr and $HOBrO_2$, and we discuss (1) the hydrolysis of $O(BrO)_2$ along a path that differs from its formation, (2) isomerization of $O(BrO)_2$ to BrO−BrO_2 followed by hydrolysis, and (3) $O(BrO)_2$ dissociation to BrO and BrO_2 and their reactions with water. The analysis shows that the rate-limiting step of HOBrO disproportionation consists of the formation of anhydride **7**, and the computed activation parameters are fully consistent with reported experimental reaction rate constants k_4.

COMPUTATIONAL METHODS

Potential energy surface (PES) analyses[30] were performed employing second-order Møller−Plesset perturbation theory

dx.doi.org/10.1021/jp301329g | J. Phys. Chem. A XXXX, XXX, XXX−XXX

(MP2)[31,32] in conjunction with the 6-311G* basis set,[33] MP2(full)/6-311G*, to locate and characterize minima and transition state structures. Selected structures were determined also with inclusion of effects of aqueous solvation at the SMD(MP2(full)/6-311G*) level, and this level is referred to as SMD for brevity. Computations were performed with *Gaussian09*[34] in conjunction with *Gaussview 5*,[35] on an SGI Altix BX2 SMP system with 64 Itanium2 processors and a Dell EM64T cluster system with 512 processors.

Solvation can be modeled by continuous and discrete solvent models,[36] and we employed a method of density-based, self-consistent reaction field theory of bulk electrostatics (SCRF), namely, the recently developed solvation model density (SMD) method.[37,38] The SMD method accounts for long-range electrostatic polarization (bulk solvent) and also for short-range effects associated with cavitation, dispersion, and solvent structural effects (CDS). The computation of the bulk effects parallels the polarizable continuum method[39,40] (PCM); it requires the dielectric constant of the solvent and the determination of the solvent accessible surface (SAS) based on atom-centered spheres with intrinsic Coulomb radii F_k. The computation of the short-range CDS term requires parameters for the atomic surface tensions (σ_k) of atoms k, for the molecular surface tension $\sigma^{[M]}$, and for the solvent accessible surface area A_k of atoms k. The atomic and molecular surface tensions depend on three solvent properties: the solvent's refractive index n, Abraham's hydrogen bond acidity parameter α, and Abraham's hydrogen bond basicity parameter β. The A_k values are computed with the knowledge of the solute atoms' van der Waal radii and the solvent radius (r_S). The SMD parametrization is based on an extensive set of 2821 solvation data including neutral and charged solutes in aqueous and nonaqueous solvents.[37]

Total energies (E_{tot}), vibrational zero point energies (*VZPE*), thermal energies (*TE*), molecular entropies (S), the numbers of imaginary frequencies (*NI*), and the lowest vibrational frequencies ν_1 and ν_2 computed for the free molecules and at the SMD level, respectively, are given in Tables S1 and S2 of the Supporting Information. In Tables 2 and 3 are listed the relative and reaction energies computed for gas phase and for aqueous solution, respectively. For each parameter, four thermodynamic values are provided, and these are ΔE, ΔH_0, ΔH_{298}, and ΔG_{298}.

RESULTS AND DISCUSSION

Structures of HOBr, HOBrO, and $HOBrO_2$. The potential energy surfaces of HBrO,[41,42] $HBrO_2$,[43,44] and $HBrO_3$[45,46] have been explored previously, mostly with a view to atmospheric chemistry. The isomers HOBr, HOBrO, and $HOBrO_2$ are pertinent in the current context and molecular models are shown in Figure 1. The structures of HOBr, HOBrO, and $HOBrO_2$ are bent at the HO-oxygen with ∠(H−O−Br) angles of 103.9°, 106.1°, and 106.9°, respectively. HOBrO adopts a nonplanar conformation **2a** with dihedral angle ∠(H−O−Br−O) = 74.2°, and the planar structures **2b** and **2c** are transition state structures for fast enantiomerization of **2a** ⇄ **2a′** (ΔE_{act}(**2a** → **2b**) = 3.0 kcal/mol; ΔG_{act}(**2a** → **2b**) = 2.3 kcal/mol). The rotational energy profile about the Br−OH bond was computed for **3**, and the anti-conformation **3a** is the only minimum. The syn-structure **3b** is a transition state structure for fast automerization of **3a** (ΔE_{act}(**3a** → **3b**) = 4.8 kcal/mol; ΔG_{act}(**3a** → **3b**) = 5.6 kcal/mol). The bond lengths between bromine and hydroxyl are d(Br−OH) ≈ 1.87 ± 0.02 Å

Table 3. Relative and Reaction Energies[a] Computed at SMD(MP2(full)/6-311G*)

eq	relation/reaction	ΔE	ΔH_0	ΔH_{298}	ΔG_{298}
R4′	E_{rxn}, 2·**2a** → **1a** + **3a**	−26.22	−26.35	−26.12	−26.04
R2″	E_{rxn}, HBr + **2a** ⇄ **21a**	−41.10	−38.88	−39.01	−40.26
R3″	E_{rxn}, HBr + **3a** ⇄ **1a** + **2a**	−14.88	−12.53	−12.89	−14.22
	E_{act}, 2·**2a** → **6b**	21.50	21.35	21.90	33.57
	E_{act}, 2·**2a** → **6c**	19.28	19.73	20.10	32.18
	E_{act}, 2·**2a** → **6e**	23.49	24.14	24.22	36.79
	E_{act}, 2·**2a** → **6f**	26.20	26.55	26.90	38.65
	7a → BrO + BrO_2	−0.93	−1.92	−2.63	−12.31
	BrO + BrO_2 → **8a**	−25.46	−23.57	−23.25	−12.98
	7a → **8a**	−26.39	−25.49	−25.87	−25.29
	E_{rxn}, 2·**2a** → **7a** + H_2O	−9.75	−11.39	−10.08	−10.23
	E_{rxn}, **1a** + **3a** → **7a** + H_2O	16.47	14.96	16.04	15.81
	E_{act}, 2·**2a** → **14a**	3.49	1.62	1.98	13.60
	E_{act}, **12a** → **14b**	5.72	2.83	2.00	3.73
	E_{act}, **7a** + H_2O → **14b**	−1.54	−1.92	−2.84	8.97
	E_{rel}, **14a** vs **14b**	14.78	14.92	14.90	14.86
	E_{act}, **1a** + **3a** → **14b**	14.93	13.04	13.20	24.78
	E_{desol}, **12a** → **7a** + H_2O	7.25	4.75	4.85	−5.24
	E_{desol}, **12b** → **7a** + H_2O	30.57	27.82	28.04	17.59
	E_{rel}, **15e** vs **14a**	4.06	5.42	5.44	5.22
	E_{act}, 2·**2a** → **15e**	7.55	7.04	7.42	18.81
	E_{desol}, **12b** → **8a** + H_2O	4.18	2.33	2.17	−7.70
	E_{rxn}, **8a** + H_2O → **1a** + **3a**	9.92	10.53	9.83	9.48
	E_{rel}, **15b** vs **15a**	3.19	4.54	4.28	5.08
	E_{rel}, **15e** vs **15a**	20.63	21.09	21.22	20.66
	E_{act}, **1a** + **3a** → **15a**	13.14	12.30	12.32	24.20
	E_{act}, **1a** + **3a** → **15b**	16.33	16.83	16.59	29.28
	E_{act}, **8a** + H_2O → **15a**	23.06	22.82	22.14	33.68
	E_{act}, **8a** + H_2O → **15b**	26.25	27.36	26.42	38.76
	E_{rxn}, **9** + **10** + H_2O → **1a** + **3a**	−15.53	−13.04	−13.42	−3.50

[a]All values are in kcal/mol.

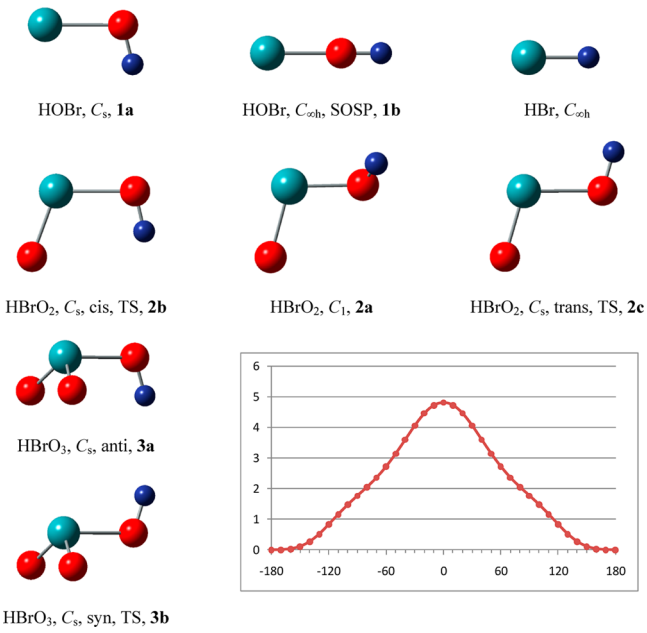

Figure 1. Optimized structures of HOBr, HOBrO, and $HOBrO_2$ and rotational energy profile of HO−BrO_2. The plot shows the relative energy (in kcal/mol) as a function of the dihedral angle ∠(H−O−Br−X) where *syn*-**3b** appears at ∠(H−O−Br−X) = 0° and *anti*-**3a** appears at ∠(H−O−Br−X) = ±180°.

dx.doi.org/10.1021/jp301329g | J. Phys. Chem. A XXXX, XXX, XXX−XXX

Table 4. Thermodynamic and Kinetic Parameters of the Disproportionation of Bromous Acid[a]

year	authors	rxn	k_n	k_{-n}	K_n	ΔG_n
1972	FKN[b]	R4	4×10^{7}	2×10^{-10}	2.0×10^{17}	−23.61
		R2	2×10^{9}	5×10^{-5}	4.0×10^{13}	−18.56
		R3	2.1	1×10^{4}	2.1×10^{-4}	5.02
1986	FF[c]	R4	3000	1×10^{-8}	3.0×10^{11}	−15.66
		R2	3×10^{6}	2×10^{-5}	1.5×10^{11}	−15.25
		R3	2.0	3.2	0.6	0.41
2012a	this work	R4	1700[d]	1.39×10^{-16}	1.22×10^{19}	−26.04[e]
"Marcus"	SMD	R2	3×10^{6}	3.64×10^{-15}	8.25×10^{20}	−28.56[f]
		R3	2.0	2.85×10^{-2}	70.08	−2.52[g]
2012b	this work	R4	1700[d]	1.39×10^{-16}	1.22×10^{19}	−26.04[e]
"Petkovic"	SMD	R2	3×10^{6}	7.33×10^{-22}	4.09×10^{27}	−36.00[h]
		R3	2.0	1.0×10^{-9}	2.00×10^{9}	−9.96[g]

[a]Reaction rate constants in M^{-1} s^{-1} for k_{-2}, k_{-3}, and k_4, in M^{-2} s^{-1} for k_2 and k_{-4}; and in M^{-3} s^{-1} for k_3. Free enthalpies in kcal/mol. [b]Table 1 in ref 25. [c]Table 2 in ref 25. [d]Reference 28. [e]Direct computation for reaction R4. [f]Computed with reaction R2″ and using Marcus's value ΔG_a(HBr) = −11.7 kcal/mol (ref 58). [g]Via $\Delta G_4 = \Delta G_2 - \Delta G_3$. [h]Computed with reaction R2″ and using Petkovic's value ΔG_a(HBr) = −4.26 kcal/mol (ref 56).

(**1a**: 1.86; **2a**: 1.88; **3a**: 1.87 Å) and roughly 0.2−0.3 Å longer than Br−O bonds (**2a**: 1.64; **3a**: 1.60 Å).

Thermochemistry of Bromous Acid Disproportionation. The computed reaction enthalpy and free reaction enthalpy of HOBrO disproportionation 2·**2a** → **1a** + **3a** are $\Delta H_4' \approx \Delta G_4' = -30.0$ kcal/mol. The estimation of the effects of aqueous solvation by computation of **1a**, **2a**, and **3a** with the SMD(MP2(full)/6-311G*) method yields $\Delta H_4'$(SMD) = −26.1 and $\Delta G_4'$(SMD) = −26.0 kcal/mol. It makes sense that the reaction entropy is close to zero for the reaction 2HOBrO ⇄ HOBr + $HOBrO_2$. The best established reaction energy for HOBrO disproportionation in aqueous media is the reaction enthalpy $\Delta H_4 = -27.2$ kcal/mol. We find that this ΔH_4 value agrees very well with $\Delta H_4'$(SMD), and this leads to a discussion of the dissociation state of bromic acid.

$$2HOBrO \rightleftarrows HOBr + HOBrO_2$$

$$(R4'),\ K_{disp} = K'_4,\ \Delta G_{disp} = \Delta G'_4$$

$$HOBrO_2 \rightleftarrows H^+ + BrO_3^- \qquad (A(\mathbf{3})),\ K_a(\mathbf{3}),\ \Delta G_a(\mathbf{3})$$

$$2HOBrO \rightleftarrows HOBr + H^+ + BrO_3^-$$

$$(R4) = (R4') + (A(\mathbf{3})),\quad K_4 = K'_4 \cdot K_a(\mathbf{3}),$$

$$\Delta G_4 = \Delta G'_4 + \Delta G_a(\mathbf{3})$$

Equilibrium Constant K_4' and Bromic Acid Dissociation. We computed the thermochemistry of reaction R4′, that is, the disproportionation of undissociated HOBrO with formation of undissociated acids HOBr and $HOBrO_2$. There exists general agreement that hypobromous acid (pK_a(HOBr) = 8.59[47]) and bromous acid (pK_a(HOBrO) = 3.43[48]) are not dissociated at the typical pH value of the BZR. In contrast, it has been assumed that bromic acid does dissociate under BZR conditions, and reaction R4 combines the disproportionation reaction R4′ with the acid dissociation reaction of bromic acid A(**3**) and hence $K_4 = K_4' \cdot K_a(\mathbf{3})$ and $\Delta G_4 = \Delta G_4' + \Delta G_a(\mathbf{3})$.

Assuming that FF's value $\Delta G_4 = -15.6_6$ kcal/mol[25] is correct, i.e., that $K_4 = k_4/k_{-4} = 3 \times 10^{+11}$ M, then one must assign the difference $\Delta G_4 - \Delta G_4' = \Delta G_a(\mathbf{3})$ to the acid dissociation reaction of bromic acid. Since $\Delta H_4'$ is very close to $\Delta H_4 = -27.2_3$ kcal/mol[28] and considering that the reaction enthalpies ΔH_a of deprotonation reactions in solution are usually positive and small in magnitude, one would be inclined to explain the difference between ΔG_4 and $\Delta G_4'$ by the entropy change associated with the acid dissociation of bromic acid and $\Delta S_a(\mathbf{3})$ would have to be negative. Qualitatively, a negative ΔS_4 value would be consistent with bromic acid dissociation, $HOBrO_2 \rightleftarrows BrO_3^- + H^+$. While acid dissociation in gas-phase increases entropy by about 23 cal/(K mol),[49] the overall entropy decrease of acid dissociation in solution is consistent with entropy reduction associated with proton solvation.[50,51]

To account for an additional reaction free enthalpy $\Delta G_{extra} = \Delta G_4 - \Delta G_4' \approx +10.3_8$ kcal/mol via the acidity of **3** would require $pK_a(\mathbf{3}) = 7.6_1$ because of $\Delta G_a(\mathbf{3}) = 2.303 \cdot RT \cdot pK_a(\mathbf{3})$. With this acidity constant, one computes the ratio $[HBrO_3]/[BrO_3^-] > 10^6$ at a typical $pH \approx 1$ of the BZ reaction, and this creates an obvious paradox. The actual $pK_a(\mathbf{3})$ value has not been well established by experimentation; values of 1.87,[52] 0.7,[53] and −0.29[54] were reported, and, most recently, Cortes and Faria concluded that $pK_a(\mathbf{3}) < -0.5$ ($\Delta G_a(\mathbf{3}) < -0.68$ kcal/mol).[55] It will be important to establish $pK_a(\mathbf{3})$ because this value decides whether one should replace reactions R3 and R4 by reactions R3′ and R4′, respectively.

$$H^+ + Br^- + HOBrO_2 \rightleftarrows HOBr + HOBrO$$

$$(R3') = (R3) + (A(\mathbf{3}))$$

$$2HOBrO \rightleftarrows HOBr + HOBrO_2 \qquad (R4')$$

With the knowledge of the range $pK_a(\mathbf{3}) = 0 \pm 1.5$ it is clear that $\Delta G_a(\mathbf{3})$ is small, and, therefore, we take the position that $\Delta G_4' = -26.0_4$ kcal/mol is close to the true ΔG_4 value, i.e., $\Delta G_4 \approx \Delta G_4'$ (Table 4). The computed value $\Delta G_4'$(SMD) gives an equilibrium constant of $K_4' = 1.22 \times 10^{+19}$ and considering the value $k_4 = 1700$ M^{-1} s^{-1} firmly established by Agreda and Field,[28] one then obtains $k_{-4} = 1.39 \times 10^{-16}$ M^{-2} s^{-1}. There has never been any doubt that reaction R4 (or R4′) is irreversible, that fact is not altered if k_{-4} is decreased by several magnitudes.

If one takes the position that $\Delta G_4 \approx \Delta G_4'$, then it also follows that $\Delta G_3 \approx \Delta G_3'$ and there are consequences for reaction R2 as well because $\Delta G_4 = \Delta G_2 - \Delta G_3$ (or $K_4 = K_2/K_3$). We computed the thermochemistry of reactions R2″ and R3″. Reactions R2 and R2″ are connected via the acid dissociation reaction A(HBr); (R2) = (R2″) − (A(HBr)), $K_2 = K_2''/K_a$(HBr), $\Delta G_2 = \Delta G_2'' - \Delta G_a$(HBr). Reactions R3″

dx.doi.org/10.1021/jp301329g | J. Phys. Chem. A XXXX, XXX, XXX−XXX

and R3′ also are connected via reaction A(HBr); (R3′) = (R3″) − (A(HBr)), $K_3' = K_3''/K_a(HBr)$, $\Delta G_3' = \Delta G_3'' - \Delta G_a(HBr)$.

$$HBr + HOBrO \rightleftarrows 2HOBr \qquad (R2'')$$

$$HBr + HOBrO_2 \rightleftarrows HOBr + HOBrO \qquad (R3'')$$

$$HBr \rightleftarrows H^+ + Br^- \qquad (A(HBr)),\ K_a(HBr),\ \Delta G_a(HBr)$$

$$H^+ + Br^- + HOBrO \rightleftarrows 2HOBr$$
$$(R2) = (R2'')\text{-}(A(HBr))$$

$$H^+ + Br^- + HOBrO_2 \rightleftarrows HOBr + HOBrO$$
$$(R3') = (R3'')\text{-}(A(HBr))$$

Free Enthalpy of HBr Dissociation and Equilibrium Constant K_2. The computed free enthalpies of reactions R2″ and R3″, respectively, are $\Delta G_2''(SMD) = -40.2_6$ kcal/mol and $\Delta G_3''(SMD) = -14.2_2$ kcal/mol, respectively. Reactions R2″ and R3″ are related to reactions R2 and R3′ via the acidity of aqueous hydrobromic acid.

Petkovic reported that the acidity of aqueous HBr is comparable to the acidity of sulfuric acid ($pK_a(HBr) = -3.12$; $pK_a(H_2SO_4) = -3.29$).[56,57] At a typical $pH \approx 1$ of a BZ reaction, one computes $[HBr]/[Br^-] \approx 10^{-4}$ and confirms the expectation that HBr is dissociated under these conditions. Petkovic's value $pK_a(HBr) = -3.12$ corresponds to $\Delta G_a(HBr) = -4.2_6$ kcal/mol. The $pK_a(HBr)$ value is not firmly established, however, and several authors have argued for a much higher acidity of HBr. The measurements by Marcus[58] resulted in the value $pK_a(HBr) = -8.6$ which corresponds to a free enthalpy of dissociation $\Delta G_a(HBr) = -11.7$ kcal/mol.

Comparison of FF's value $\Delta G_2 = -15.2_5$ kcal/mol to the computed value $\Delta G_2''(SMD) = -40.2_6$ kcal/mol leads to $\Delta G_a(HBr) = -25.0_1$ kcal/mol. The computed value $\Delta G_2''(SMD) = -40.2_6$ kcal/mol can be associated with an error of a few kcal/mol, but an error as high as 10 kcal/mol does not seem likely. Hence, assuming that $\Delta G_2''(SMD)$ is essentially correct (i.e., within a couple of kcal/mol) and with Marcus's value $\Delta G_a(HBr) = -11.7$ kcal/mol, we arrive at the estimate $\Delta G_2 = -28.5_6$ kcal/mol and the corresponding equilibrium constant $K_2 = 8.25 \times 10^{+20}$ M^{-1} (Table 4, 2012a). The respective values computed with Petkovic's value $\Delta G_a(HBr) = -4.2_6$ kcal/mol also are included in Table 4 (2012b).

Coupled Reactions and Equilibrium Constant K_3'. Reactions R2, R3, and R4 are coupled because $\Delta G_4 = \Delta G_2 - \Delta G_3$ and $K_4 = K_2/K_3$. The FKN values $K_2 = 4.0 \times 10^{13}$ M^{-1}, $K_3 = 2.1 \times 10^{-4}$ M^{-2}, and $K_4 = 2.0 \times 10^{17}$ M (very nearly) fulfill this condition (Table 4). The FF values $K_2 = 1.5 \times 10^{11}$ M^{-1} and $K_4 = 3 \times 10^{11}$ M also fulfill this condition if $K_3 = 0.5$ M^{-2} (rather than 0.6) corresponding to $\Delta G_3 = 0.4_1$ kcal/mol. With the value $\Delta G_4' = -26.0_4$ kcal/mol and using either $\Delta G_2 = -28.5_6$ kcal/mol ("Marcus") or $\Delta G_2 = -36.0_0$ kcal/mol ("Petkovic"), respectively, one arrives at the $\Delta G_3'$ values of −2.5 or −10 kcal/mol, respectively.

Dimeric Aggregates of Bromous Acid, $(HOBrO)_2$. Molecular models of dimeric aggregates **4** of bromous acid are shown in Figure 2, and they include 4-, 6-, and 8-membered ring structures. The aggregation hardly affects intramolecular bonding (e.g., bond lengths[59] are $d(Br{-}OH) \approx 1.87 \pm 0.10$ Å and $d(Br{-}O) \approx 1.66 \pm 0.02$ Å in dimers **4**), and only selected intramolecular bonding parameters are described.

The most stable dimer of HOBrO adopts an eight-membered ring structure **4a** held together by two OH···O hydrogen bonds

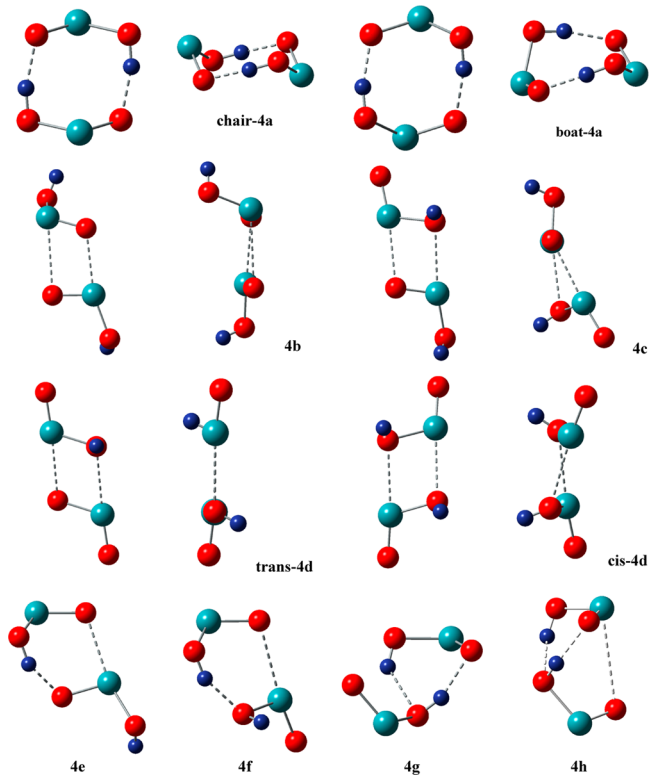

Figure 2. Optimized structures of dimeric aggregates of HOBrO, **4**.

(chair-**4a**: 1.67 Å; boat-**4a**: 1.72 Å), and the chair conformation is slightly preferred over the boat conformation ($\Delta E = 2.9$ kcal/mol; $\Delta G = 2.2$ kcal/mol). The reaction energies computed for the dimerization 2·**2a** → chair-**4a** ($\Delta E_{dim} = -27.2$ kcal/mol; $\Delta G_{dim} = -12.4$ kcal/mol) show the strength of the OH···O bonds in **4a**.

Dimer **4a** might be important as the resting state of HOBrO, but it is not a suitable substrate for O-transfer between two Br centers. A substrate for direct O-transfer should contain at least one intermolecular BrO···Br contact. This is easily realized in dimer **4b**, that is, the four-membered ring structure with two BrO···Br contacts (2.67 and 3.12 Å) and antiparallel alignment of the large dipole moments of the BrO bonds. Note that the HOBrO molecules in **4b** are not equivalent; the BrO_2 planes of the two molecules are nearly perpendicular, and one can describe their interaction as a T-contact.[60] The tautomeric aggregate **4c** involves the BrO bond of one HOBrO and the BrO(H) bond of another and features one BrO···Br halogen bond (2.84 Å) and one BrO(H)···Br halogen bond (2.82 Å). Substrate **4c** would allow for two disproportionation paths: Direct O-transfer to form HOBr and $HOBrO_2$ or indirect O-transfer involving OH-transfer (i.e., formation of contact ion pair $[(HO)_2BrO]^+BrO^-$) and subsequent tautomerization. The consideration of this type of indirect O-transfer adds dimer **4d** to the palette of putative reactive substrates. Aggregate **4d** involves antiparallel alignment of the BrO(H) bonds of two HOBrO molecules, allows for cis and trans stereoisomers, and features two BrO(H)···Br halogen bonds (trans: 2.89 Å, cis: 2.86 Å). As can be seen from the entries in Table 2, the four-membered ring aggregates **4b**, **4c**, and **4d** all are rather close in energy and significantly less stable than chair-**4a** ($\Delta E_{rel} = 18.5 \pm 0.5$ kcal/mol and $\Delta G_{rel} = 14.9 \pm 0.5$ kcal/mol).

In addition, we considered three cyclic dimers with six-membered ring skeletons, and these structures are attractive

dx.doi.org/10.1021/jp301329g | J. Phys. Chem. A XXXX, XXX, XXX−XXX

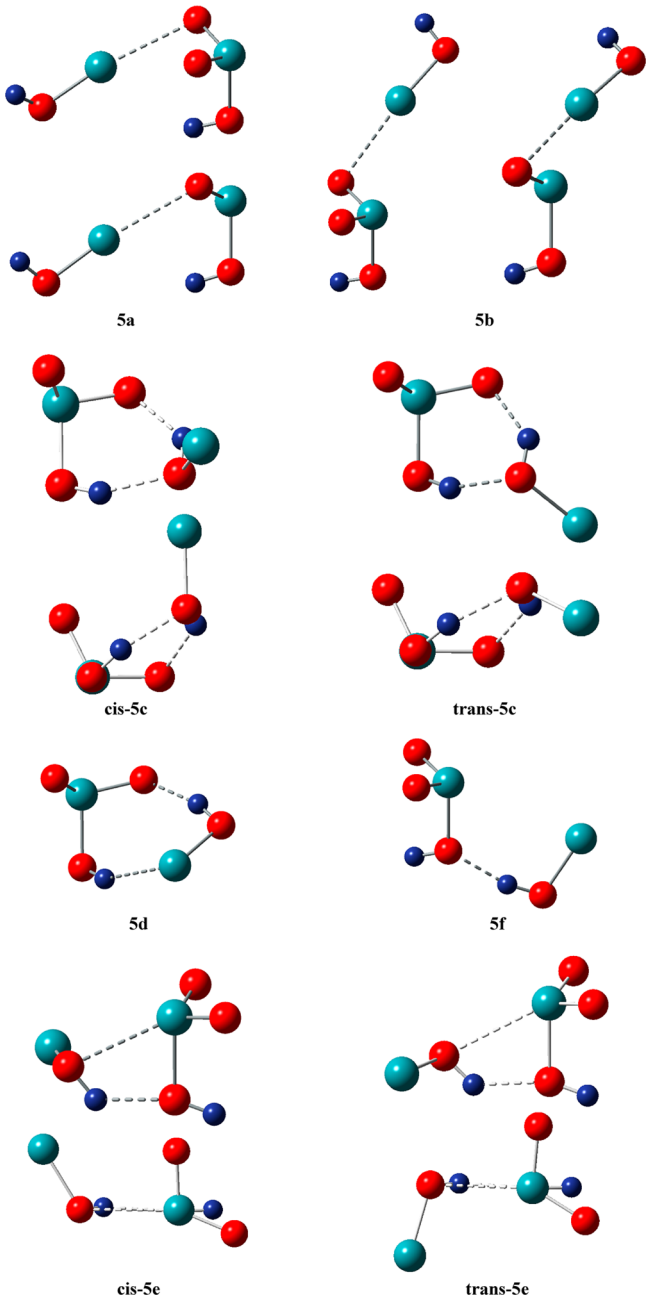

Figure 3. Optimized structures of the $(HBrO_3)(HOBr)$ aggregate **5**. The models for the cis and trans isomers of **5c** and **5e** also are shown as Newman projections along the Br−OH bond of the HO−BrO_2 moiety. Note that the OH group is in front in the Newman projections of cis-**5c** and trans-**5c**, while it is in back in the Newman projections of cis-**5e** and trans-**5e**.

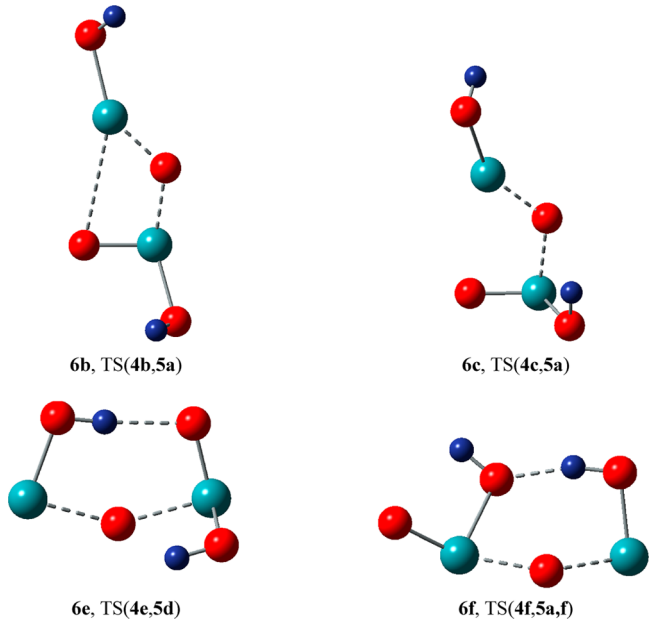

Figure 4. Optimized structures of O-transfer transition state structures **6**.

options because of the absence of significant ring strain. Two of these dimers are held together by one BrOH···O hydrogen bond (**4e**: 1.79 Å; **4f**: 1.83 Å) and one BrO···Br halogen bond (**4e**: 2.59 Å; **4f**: 2.78 Å), and the third structure **4g** features two BrOH···O hydrogen bonds. In structures **4e** and **4f**, the halogen bond must be of the BrO···Br type, and the hydrogen bond may use an O- or an OH-acceptor, respectively. The formations of **4e**-**4g** are much more exothermic compared to **4b**-**4d**, and these cyclic aggregates even remain exergonic in gas-phase.

Mixed Aggregate of Bromic Acid and Hypobromous Acid, $(HOBrO_2)(HOBr)$. The product of disproportionation by direct O-transfer is the mixed molecular aggregate $(HOBrO_2)$-(HOBr), and possible structures are shown in Figure 3. Aggregates **5a** and **5b** both contain one HOBr···OBr(O)OH halogen bond (**5a**: 2.84 Å; **5b**: 2.87 Å), and they differ as to whether HOBr and the OH group of $HOBrO_2$ are on the same or on opposite sides of the BrO_2 plane. In **5a**, there might exist the possibility for an HOBr···$HOBrO_2$ hydrogen bonding interaction (2.91 Å). Considering the relative energies computed for **5a** and **5b**, however, it is clear that the halogen bonding is the dominant intermolecular interaction. The aggregation energies for **5a** and **5b** are exothermic but endergonic.

Aggregates cis-**5c** and trans-**5c** contain two O···HO hydrogen-bonds with $HOBrO_2$ acting as HB-donor (cis: 1.84 Å; trans: 1.85 Å) and HB-acceptor (cis: 1.96 Å; trans: 1.94 Å). Aggregate **5d** also contains two H-bonds, but bromine is now one of the acceptors. The O···HO bond (1.88 Å) uses HOBr as HB-donor, and a BrO-acceptor and the Br···HO bond (2.66 Å) uses HOBr's bromine as HB-acceptor. The main interaction in aggregates **5e** and **5f** is one O···HO bond which uses HOBr as HB-donor and BrO(H) as HB-acceptor (**5e**: 1.96 Å; **5f**: 1.81 Å). The geometry of **5e** would allow for a secondary BrO contact (2.92 Å). Among the H-bonded aggregates **5c**-**5f**, the isomers of **5c** are bound the most, but even these aggregates remain endergonic in the gas-phase.

Transition State Structures for Direct O-Transfer. Several transition state structures **6** (Figure 4) were located for direct O-transfer within dimeric aggregates **4**, and the letter descriptor of **6** matches the respective descriptor of its "dimer substrate" (Figure 2). Hence, **6b**, **6c**, **6e**, and **6f**, respectively, are the transition state structures associated with O-transfer within **4b**, **4c**, **4e**, and **4f**, respectively, and leading to product aggregates **5a**, **5a**, **5d**, and cis-**5c**, respectively.

The activation energies for the O-transfer reaction via the four-membered ring transition state structures **6b** and **6c** do not appear to suffer from ring strain: $E_{act}(2\cdot\mathbf{2a} \rightarrow \mathbf{6b})$ = 16.7 kcal/mol and $E_{act}(2\cdot\mathbf{2a} \rightarrow \mathbf{6c})$ = 13.9 kcal/mol are comparable to activation energies $E_{act}(2\cdot\mathbf{2a} \rightarrow \mathbf{6f})$ = 18.6 kcal/mol and $E_{act}(2\cdot\mathbf{2a} \rightarrow \mathbf{6e})$ = 15.1 kcal/mol for O-transfer via the six-membered ring transition state structures. All of these reactions

dx.doi.org/10.1021/jp301329g | J. Phys. Chem. A XXXX, XXX, XXX−XXX

Scheme 1. Mechanistic Options for the Disproportionation 2HOBrO ⇄ HOBr + $HOBrO_2$ by Direct O-Transfer and via Condensation-Hydration Sequences Involving $O(BrO)_2$[a]

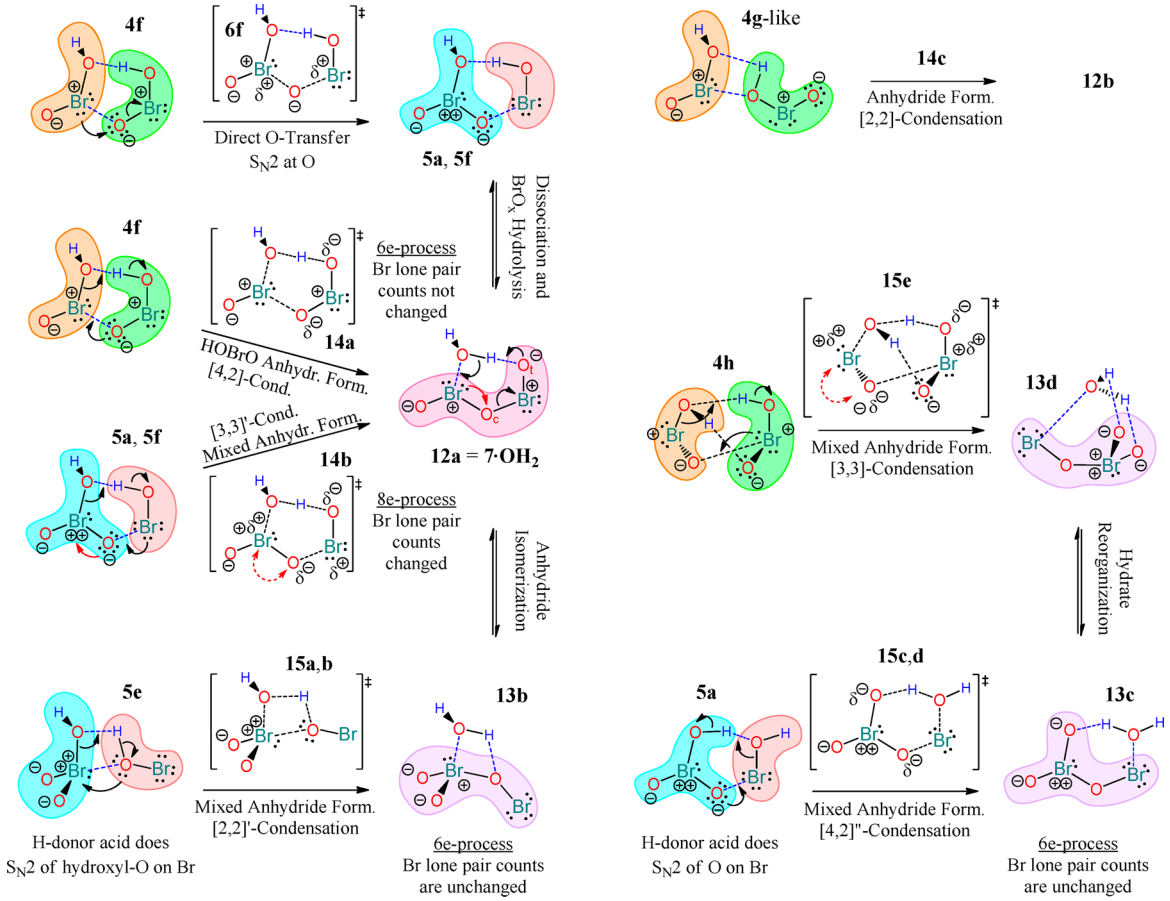

[a]Options for the latter include direct hydrolysis of $O(BrO)_2$, isomerization of $O(BrO)_2$ to $BrO-BrO_2$ followed by hydrolysis, and $O(BrO)_2$ dissociation to BrO and BrO_2 and their reactions with water.

require organization in the transition state region, and the activation free enthalpies are high and above 27 kcal/mol. We also determined the transition state structures **6b**, **6c**, **6e**, and **6f** for direct O-transfer at the SMD level, and the effects of aqueous solvation increase the activation energies above 19 kcal/mol and the activation free enthalpies above 32 kcal/mol.

If Not Direct O-Transfer, Then What? Direct O-transfer is possible between two molecules of bromous acid, but the activation barriers all are too high compared to measured data for the disproportionation of bromous acid. Direct O-transfer is exemplified in Scheme 1 together with mechanistic alternatives for indirect O-transfer by way of condensation and hydration sequences. To facilitate the discussion, all Lewis structures in Scheme 1 are drawn with polar BrO bonds (Br^+-O^- instead of Br=O). This convention has the advantage that the lone pair count at bromine immediately informs about a change in the oxidation state of bromine during a reaction. We do show all lone pairs at bromine in Scheme 1, while we usually omit lone pairs on oxygen. Blue dashed lines are used to indicate intermolecular interactions (H-bonding, halogen bonding), whereas black dashed lines in Lewis structures of transition state structures indicate bonds that are being formed or broken during the reaction.

Direct O-transfer is exemplified in the first row of Scheme 1 to the left, and it requires nucleophilic substitution at oxygen by a poor bromine nucleophile, the further oxidation of the same already electron-deficient bromine, and the reduction of the bromine of the leaving group BrOH. We illustrate the direct O-transfer mechanism with aggregate **4f** for a good reason: Searches for the O-transfer transition state associated with **4f** on occasion led to a region of the potential energy surface that corresponds to the hydrate of dibromotrioxide, $O(BrO)_2$. This condensation reaction is illustrated in the second row of Scheme 1, and one of its advantages becomes immediately obvious: it is a nucleophilic substitution at bromine by a good nucleophile and intramolecular leaving group stabilization by way of proton transfer.

In the following, we first present a discussion of the potential energy surface of Br_2O_3 and show that $O(BrO)_2$ is prone to isomerization to $BrO-BrO_2$ and to dissociation to BrO and BrO_2. Hence, there are three possible paths from $O(BrO)_2$ to the products of disproportionation, HOBr and $HOBrO_2$, and these will be discussed: (1) hydrolysis of $O(BrO)_2$ along a path that differs from its formation, (2) isomerization of $O(BrO)_2$ to $BrO-BrO_2$ followed by hydrolysis, and (3) $O(BrO)_2$ dissociation to BrO and BrO_2 and their reactions with water.

Dibromotrioxide $O(BrO)_2$, Radicals BrO and BrO_2, and Mixed Anhydride $BrO-BrO_2$. The bromous acid anhydride prefers the C_2-symmetric structure **7a**, and C_s-**7b** is a local minimum about 1.5 kcal/mol higher in energy (Figure 5). The PES scan of Br_2O_3 as a function of the ∠(Br−O−Br−O_t)

dx.doi.org/10.1021/jp301329g | J. Phys. Chem. A XXXX, XXX, XXX−XXX

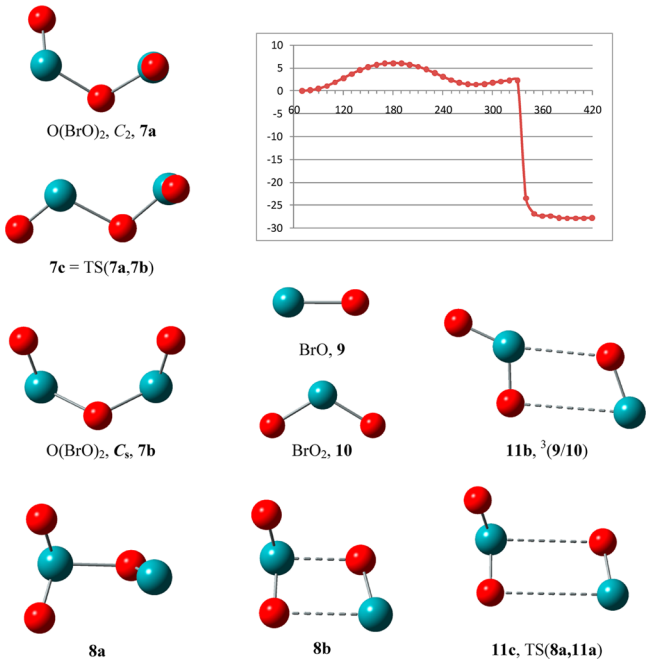

Figure 5. Rotational energy profile and optimized structures of bromous acid anhydride OBr−O−BrO, **7**, stationary structures of mixed anhydride BrO−BrO_2, **8**, and structures of free and paired radicals BrO_x. The plot shows the relative energy (in kcal/mol) as a function of the dihedral angle ∠(Br−O−Br−O) starting with the value in **7a**.

dihedral angle shows that **7a** is easily converted to **7b** via the rotational transition state structure **7c** = RTS(**7a**,**7b**) with a barrier of about 5−6 kcal/mol. The scan shows a discontinuity in the region where the dihedral angle ∠(Br−O−Br−O_t) comes close to zero. Once **7** enters the region of the **7b** conformation, the pure anhydride **7** collapses to the mixed anhydride **8a**, BrO−BrO_2, with a BrO−BrO_2 bond length of 2.02 Å. We also explored the potential energy surface of **7** as a function of the OBr−OBrO bond while constraining both ∠(Br−O−Br−O_t) dihedral angles to their values in **7a**. Again, the structure collapsed to the mixed anhydride around d(OBr−OBrO) ≈ 2.35 Å and with a tiny barrier of less than 3.5 kcal/mol. It is possible that the collapse of **7** leads through thermally nonequilibrated **8**-type structures to more or less free radicals BrO and BrO_2.

The homolysis of **7a** to the free radicals BrO, **9** and BrO_2, **10** is slightly exothermic (ΔH_{298} = −2.3 kcal/mol) and more exergonic (ΔG_{298} = −12.1 kcal/mol). Whether the rearrangement **7a** → **8a** will occur depends on the properties of the singlet radical pair (BrO)(BrO_2), ^{1}**11a**. The radical recombination **9** + **10** → **8** to the mixed anhydride certainly is an option because it is exothermic (ΔH_{298} = −25.1 kcal/mol) enough to also be exergonic (ΔG_{298} = −15.1 kcal/mol). Overall, the isomerization **7a** → **8a** is highly exergonic by ΔG_{298} = −27.1 kcal/mol and de facto irreversible.

We then located the transition state structure **8b** with d(BrO−BrO_2) = 2.29 Å, and **8b** is only slightly less stable that **8a**. The transition vector of **8b** shortens the BrO···BrO_2 bond and lengthens the OBr···OBrO bond, and **8b** looks like the transition state structure for isomerization of **7** and **8**. However, **8b** is more stable than **7a**, and, hence, **8b** must function as a transition state structure for the dissociation of **8a** to BrO and BrO_2. The triplet radical pair ^{3}**11b** formed between **9** and **10** shows an OBr bond length of 3.05 Å; it is bound by ΔH_{298} = 2.6 kcal/mol, but the association is endergonic by ΔG_{298} = 3.4 kcal/mol, respectively. We located a transition state structure **11c** with a BrO−BrO_2 bond length of 3.39 Å, and energy of ΔG_{298} = −6.6 kcal/mol relative to free **9** and **10**, and its imaginary mode shows the motion from radical pair to form **8a**.

The SMD model shows that all the essential features of the gas-phase potential energy surface carry over to aqueous solution, and, moreover, the solvation effects alter the thermodynamic reaction parameters less than 2 kcal/mol (Table 3). In particular, the homolysis **7a** → BrO + BrO_2 is exergonic by ΔG_{298}(SMD) = −12.3 kcal/mol, the radical combination reaction BrO + BrO_2 → **8a** also is exergonic by ΔG_{298}(SMD) = −13.0 kcal/mol, and overall the isomerization reaction **7a** → **8a** reaction is exergonic by ΔG_{298}(SMD) = −25.3 kcal/mol.

Bromous Acid Dimers and Dibromotrioxide Hydrates. The optimized structure of C_2-**7a** is perfectly set up for one H-bond and one bromine−oxygen contact in the hydrate Br_2O_3·OH_2, **12a** = **7a**·OH_2 (Figure 6), but water binding is only slightly exergonic (ΔH_{298} = −11.5, ΔG_{298} = −1.2 kcal/mol) nevertheless. We located the transition state structure **14a** for the dimerization of HOBrO with water condensation. Alternatively, **14a** can be viewed as the transition state structure for 1,4-addition of water to $O(BrO)_2$ with concomitant Br−O bond cleavage to form the HOBrO dimer **4f**. The reaction

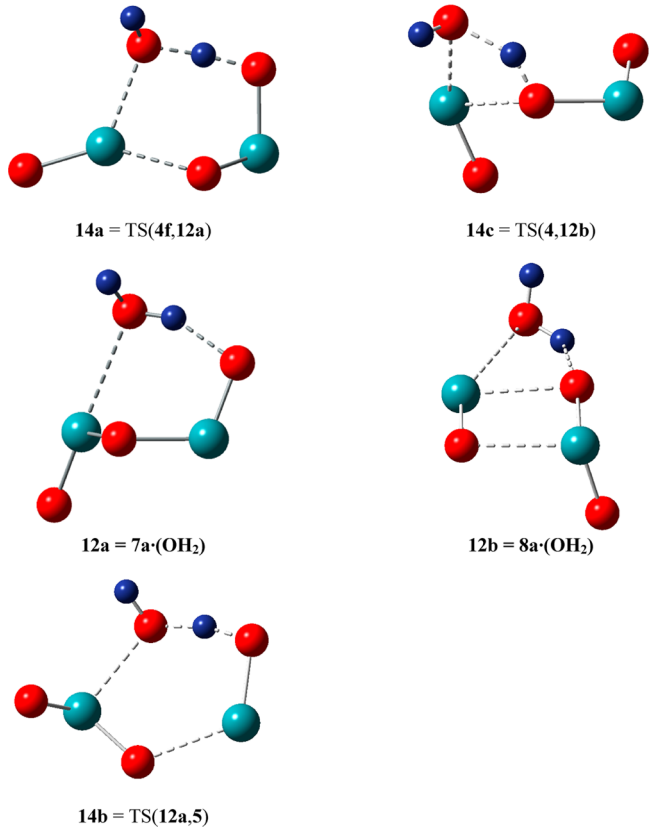

Figure 6. Optimized structure of hydrate **12a** of anhydride **7a**, of transition state structure **14a** for its formation from two HOBrO molecules, and of transition state structure **14b** for its hydrolysis to HOBr and $HOBrO_2$. The transition state structure **14c** for potential [2,2]-condensation of two HOBrO molecules actually leads to mixed anhydride **8**.

dx.doi.org/10.1021/jp301329g | J. Phys. Chem. A XXXX, XXX, XXX−XXX

energies for the reactions **4f** ⇄ **12a** and 2HOBrO ⇄ **7a** + OH_2 both are exothermic and exergonic by about 10 kcal/mol in gas-phase. Importantly, the activation barrier for the water elimination is significantly *lower* than for any of the direct O-transfer paths. The process **4f** → **14a** requires activation of ΔH_{298} = 7.7 and ΔG_{298} = 8.9 kcal/mol, and the activation energies for the process 2·**2a** → **14a** are ΔH_{298} = −5.2 and ΔG_{298} = 6.8 kcal/mol. The results of the SMD computations show that the condensation reaction 2HOBrO ⇄ **7a** + H_2O again is exothermic and exergonic by about 10 kcal/mol in aqueous solution. However, the activation energies for the process 2·**2a** → **14a** are raised by about 7 kcal/mol, and they are ΔH_{298}(SMD) = 2.0 and ΔG_{298}(SMD) = 13.6 kcal/mol.

Scheme 1 shows how anhydride **7** is formed by condensation of two HOBrO molecules via transition state structure **14a**, and **7** can therefore be seen as a "symmetrical anhydride" (i.e., *R* = R′ in R−CO−O−CO−R′). However, **7** also can be seen as a "mixed anhydride" formed by condensation of HOBr and $HOBrO_2$ although it might not be trivial to recognize this option because a "mixed anhydride" usually is unsymmetric (i.e., a mixed carboxylic acid anhydride with R ≠ R′ in R−CO−O−CO−R′). We located transition state structure **14b** (Figure 6), and it is only slightly less stable than **12a**: The activation energies for the process **12a** → **14b** are ΔG_{298} = 1.9 kcal/mol and ΔG_{298} = 3.7 kcal/mol at the MP2 and SMD levels, respectively. For the process **7a** + H_2O → **14b** the ΔG_{298} values are 0.7 and 9.0 kcal/mol at the MP2 and SMD levels, respectively. No matter what the reference, the transition state structure **14b** is much more stable than **14a** (by about 15 kcal/mol), and, hence, the formation of the "symmetrical anhydride" from bromous acid becomes an irreversible reaction for all practical purposes because **7** will instead be hydrolyzed as a "mixed anhydride" to afford HOBr and $HOBrO_2$ in an exothermic and exergonic reaction.

The reaction **12a** → [**14b**] → **5** begins with proton transfer from water to the terminal O_t atom (d(OH) = 1.149 Å in **14b**) and the heterolysis of the proximate O_c−BrO_t bond (2.606 Å in **14b**) rather than heterolysis of the remote Br−O_cBrO_t bond (as in **14a**). The heterolysis of the proximate O_c−Br bond shifts the electron pair to Br and creates an incipient electron hole at O_c. Hence, the O_c−Br heterolysis creates a strong incentive for Br→O_c electron transfer and the formation of the new Br−OH bond (2.361 Å in **14b**).

Classification of Br_2O_3 Anhydride Formations. A condensation path must involve the cleavage of a Br−OH bond of one substrate (the OH donor) and the transfer of an H atom from the other substrate (the H-donor). These constraints allow for a variety of mechanisms depending on the location of the newly formed bond. In **14a**, for example, the H-donor reacts as a 1,4-reagent, that is, the new intermolecular bond is formed with the atom that is in position 4 relative to H in the H-donor substrate. In this reaction, the OH-donor reacts as a 1,2-reagent, that is, the new intermolecular bond is formed with the atom that is in position 2 relative to hydroxyl-O in the OH-donor substrate. The mechanisms of condensation reactions between an H-donor 1,*n*-reagent and an HO-donor 1,*m*-reagent thus can be described as [*n*,*m*]-condensations. Hence **14a** is the transition state structure of a [4,2]-condensation of two HOBrO molecules.

This classification allows for a systematic evaluation of the options for the condensation of two molecules of bromous acid. The [2,3]- and [4,3]-condensations would lead to products with an O−O bond, and [3,2]-condensations would lead a product with a Br−Br bond; neither of these options were explored. On the other hand, a [2,2]-condensation reaction of two HOBrO molecules might lead to **7** via transition state structure **14c**, and, importantly, there also exists a path for [3,3]-condensation of two HOBrO molecules via transition state structure **15e** for the direct formation of mixed anhydride **8**.

This same type of classification can be applied to the formations of mixed anhydrides in conjunction with a specification as to whether HOBr is the H-donor (primed) or the HO-donor (double-primed). Thus, **14b** is the transition state structure of a [3,3]′-condensation. Aside from the formation of **7** by [3,3]′-condensation via transition state structure **14b**, we explored two modes for [2,2]′-condensation of HOBr and $HOBrO_2$ via transition state structures **15a** and **15b**, respectively, and two modes of [4,2]"-condensation via transition state structures **15c** and **15d**, respectively.

Bromous Acid [2,2]-Condensation and [3,3]-Condensation. The transition state structure **14c** for [2,2]-condensation of two HOBrO (Figure 6) looks as expected for a condensation to form **7** (Scheme 1, top right). We searched the potential energy surface for the hydrate of the symmetrical anhydride **7a**, the expected product, but the searches led directly to structure **12b** which really is a hydrate of **8** (Figure 6) with a solvation energy of ΔG_{298} = 4.9 kcal/mol. It is an interesting structural feature of **12b** that the bond lengths d(BrO−BrO_2) = 2.499 Å and d(BrO−OBrO) = 2.496 Å are almost equal; i.e., the mere presence of a water molecule results in a Br_2O_3 moiety that is neither the symmetrical nor the unsymmetrical anhydride. Most importantly, we find that the activation energy for the [2,2]-condensation 2·**2a** → [**14c**] → **12b** is ΔG_{298} = 26.7 kcal/mol and that it is much higher than for the [4,2]-condensation 2·**2a** → [**14a**] → **12a**.

The transition state structure **15e** for [3,3]-condensation of two HOBrO molecules affects the direct formation of mixed anhydride **8** (Scheme 1, center right). A molecular model of **15e** is included in Figure 7, and we will discuss its structure below in comparison to **15d**. Most importantly, **15e** *is significantly less stable than* **14a** at the MP2 and SMD levels, and the relative free enthalpies of ΔG_{298} = 5.2 kcal/mol happen to be the same at the two levels. This energy difference between **15e** and **14a** is quite consequential for the chemistry, and indeed bromous acid disproportionation would not be possible otherwise. The *much more* exergonic formation of the unsymmetrical anhydride **8** is kinetically hindered, and the symmetrical anhydride **7** is formed instead. The symmetrical anhydride **7** can be hydrolyzed to HOBr and $HOBrO_2$ in an exergonic reaction and with little activation energy, while the mixed anhydride **8** cannot.

Formation of Anhydrides from HOBr and $HOBrO_2$. As discussed above, the [3,3]′-condensation affords the formation of hydrate **12a** of symmetrical anhydride **7** from aggregate **5** via **14b** (Scheme 1, third row). The forward reaction formally involves nucleophilic addition of a weak bromine nucleophile to an anionic oxygen of **3a** with concomitant O→Br electron transfer within the **3a** moiety (dashed red arrow in Scheme 1). In a way, the intramolecular O→Br electron transfer allows for the retention of the existing Br−O bond in **3a** as the new O−Br bond to **1a** is formed. The formation of the symmetrical anhydride via **1a** + **3a** → **7a** + H_2O is endothermic and endergonic at the MP2 and SMD levels (ΔG_{298} = +20.0 kcal/mol, ΔG_{298}(SMD) = +15.8 kcal/mol), whereas the formation of the mixed anhydride **1a** + **3a** → **8a** + H_2O is exothermic and

dx.doi.org/10.1021/jp301329g | J. Phys. Chem. A XXXX, XXX, XXX−XXX

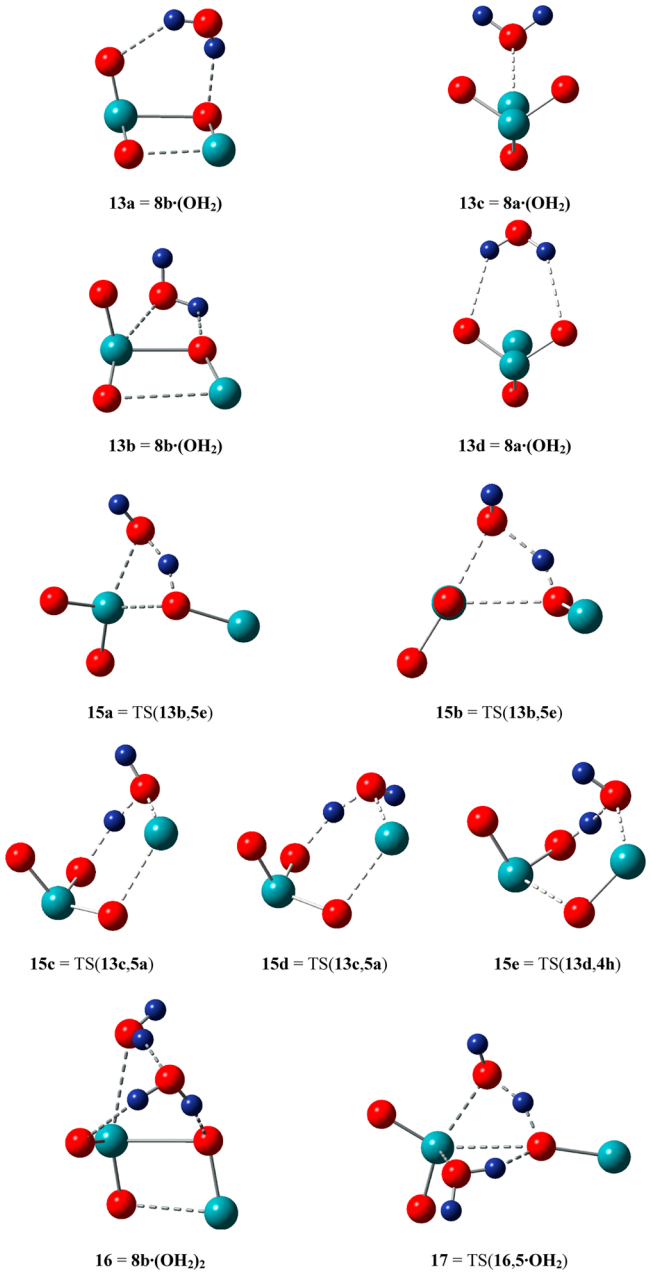

Figure 7. Optimized structures of hydrate **13** of anhydride **8** and of transition state structures for hydrolysis of **8** to HOBr and $HOBrO_2$. The transition state structures **15e** for [3,3]-condensation of two HOBrO also leads to **8**.

exergonic at the MP2 and SMD levels (ΔG_{298} = −7.2 kcal/mol; ΔG_{298}(SMD) = −9.5 kcal/mol). Hence, the question remains whether HOBr might react with $HOBrO_2$ to form the mixed anhydride.

Two types of mechanisms for condensations leading to hydrates **13** of the unsymmetrical anhydride **8** are illustrated in the bottom row of Scheme 1. We located hydrates **13a**−**13d** of mixed anhydride **8** (Figure 7). There are two H-bonds in structure **13a**, hydrate **13b** is perfectly setup to form one H-bond with the OBr moiety and one bromine−oxygen contact with the BrO_2 moiety, hydrate **13c** features one bromine−oxygen contact with the terminal bromine, and **13d** is a stereoisomer of **13c** with one less H-bond. The formation reactions of hydrate **13a**, **13c**, and **13d** are endergonic (**13a**: ΔH_{298} = −5.9; ΔG_{298} = +4.3 kcal/mol; **13c**: ΔH_{298} = −7.0; ΔG_{298} = +3.7 kcal/mol; **13d**: ΔH_{298} = −3.2; ΔG_{298} = +5.6 kcal/mol), while the formation of **13b** is almost thermoneutral (ΔH_{298} = −9.9; ΔG_{298} = 0.1 kcal/mol).

The HOBr molecule is the H-donor in [2,2]′-condensation, and we located two stereoisomeric transition states **15a** and **15b** for the formation of hydrate **13b** (Figure 7) with very similar energy. There is a small ΔG_{298} preference for **15a**, and we discuss **15a**. Even though the condensation **1a** + **3a** → **8a** + H_2O is exothermic and exergonic while the condensation **1a** + **3a** → **7a** + H_2O is greatly endothermic and endergonic, the activation barriers for the symmetrical and unsymmetrical anhydride formations are quite similar at the MP2 level with values of ΔG_{298}(**1a** + **3a** → [**14b**]‡) = 20.7 kcal/mol and ΔG_{298}(**1a** + **3a** → [**15a**]‡) = 22.8 kcal/mol. At the SMD level, the activation barriers are even closer and with a small preference for the formation of **8**; ΔG_{298}(**1a** + **3a** → [**14b**]‡) = 24.8 kcal/mol and ΔG_{298}(**1a** + **3a** → [**15a**]‡) = 24.2 kcal/mol.

Hypobromous acid HOBr is the HO-donor in [4,2]”-condensation, and we located two stereoisomeric and almost isoenergetic transition states **15c** and **15d** for the formation of hydrate **13c** (Figure 7). These transition state structures are much higher in energy than **15a** or **15b**, and, clearly, [4,2]”-condensation cannot compete with [2,2]′-condensation.

Hydrolysis of Mixed Anhydride. Suppose mixed anhydride **8a** was formed by isomerization of **7a** or by combination of radicals BrO and BrO_2. Would it be possible to hydrolyze the mixed anhydride to HOBr and $HOBrO_2$? The reaction energies for the reactions **13b** ⇄ **5e** and **8a** + H_2O ⇄ **1a** + **3b** both are endothermic and endergonic by about 7−11 kcal/mol. The process **13b** → **15a** requires activation of ΔH_{298} = 28.3 and ΔG_{298} = 29.9 kcal/mol, and the activation energies for the process **8a** + H_2O → **15a** are ΔH_{298} = 18.5 and ΔG_{298} = 30.0 kcal/mol. At the SMD level the reaction **8a** + H_2O ⇄ **1a** + **3b** is endergonic by ΔG_{298}(SMD) = 9.5 kcal/mol, and the activation free enthalpy is ΔG_{298}(SMD) = 33.7 kcal/mol.

We also considered the dihydrate **16** formed by the coordination of **8** by water molecules in both of the positions occupied in **13a** and **13b**. The activation barrier for the hydrolysis of **16** via the transition state structure **17** again is $\Delta G_{act} \approx$ 30.0 kcal/mol, and the path remains inaccessible.

These results show that the hydrolysis of the mixed anhydride **8** is kinetically hindered and that a thermally equilibrated **8** cannot be on the reaction path for disproportionation.

Reactions of BrO_x Radicals with Water. Finally, anhydride **7** might collapse to radicals BrO and BrO_2 without formation of **8**, and one must ask whether the radicals BrO_x could result in the formations of HOBr and $HBrO_3$. Buxton and Dainton generated BrO (Δ_{max} = 350 nm) and BrO_2 (λ_{max} = 475 nm) separately and monitored their disproportionations in water,[61] but the reaction rates of BrO_x hydrolyses at lower pH values are not known. The computations show that the H-transfer reactions BrO + H_2O → **1a** + HO and BrO_2 + H_2O → **2a** + HO both are endergonic and that the H-abstraction from water is much easier for BrO than for BrO_2. Guha and Francisco[62] studied the H-abstraction from HOBrO by OH, and their best reaction enthalpy (QCISD(T)//MP2 level with well polarized basis sets) agrees closely with ours. The addition reactions BrO + HO → **2a** and BrO_2 + HO → **3b** both are exergonic, and the reaction free enthalpy of the latter is slightly more exergonic. If both radicals BrO and BrO_2 are present in close proximity, one can imagine that BrO would perform most

dx.doi.org/10.1021/jp301329g | J. Phys. Chem. A XXXX, XXX, XXX−XXX

of the H-abstractions to form HOBr and that BrO_2 would add hydroxyl to generate $HBrO_3$ and the overall reaction BrO + BrO_2 + H_2O → **1a** + **3b** is exergonic (Tables 2 and 3).

We determined the transition state structures **18** and **19** for H-transfer from water to BrO and BrO_2, respectively, and we also determined the transition state structure **20** for H-transfer in the dihydrate of BrO (Figure 8). As expected, the activation

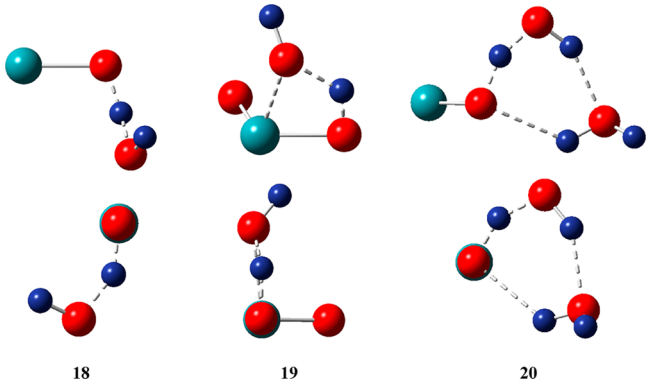

Figure 8. Optimized structures of transition state structures **18** and **19** for H-transfer from water to BrO and BrO_2, respectively. Structure **20** is the transition state structure for H-transfer in the dihydrate of BrO.

barrier for H-abstraction is much lower for BrO than for BrO_2 (Table 2), but all of the activation barriers for H-abstraction are about 30 kcal/mol or higher.

Reaction Rate Constant of HOBrO Disproportionation. The results of our study show that the rate-limiting step of the reaction 2HOBrO → HOBr + $HOBrO_2$ consists of the condensation reaction 2HOBrO → OBr−O−BrO + H_2O. The activation barrier for this reaction is almost entirely due to the entropy term; ΔS_{act} = −40.0 cal K^{-1} mol^{-1} and ΔS_{act}(SMD) = −39.0 cal K^{-1} mol^{-1}. Note that the activation enthalpy is slightly negative[63] in gas-phase (ΔH_{act} = −5.2 kcal/mol) and that the respective values are positive but small in aqueous solution (ΔH_{act}(SMD) = +2.0 kcal/mol).

With the Eyring equation[64] $k_4 = (k_B \cdot T/h)\exp(-\Delta G_{act}/RT)$, the computed activation free enthalpy ΔG_{act}(SMD) = 13.6 kcal/mol returns the reaction rate constant k_4 = 667.5 M^{-1} s^{-1}. With error bars of ±1 or ±2 kcal/mol, respectively, the computed rate constant falls in the ranges 123.4 M^{-1} s^{-1} < k_4 < 3610 M^{-1} s^{-1} or 22.8 M^{-1} s^{-1} < k_4 < 19,519 M^{-1} s^{-1}, respectively. This result is in full agreement with the experimental studies by Sullivan and Thompson,[22] Noszticzius et al.,[23] Ariese and Nagy-Ungvirai,[24] Field and Försterling,[25] and the most recent study by Agreda and Field.[28]

We can also compare the computed activation free enthalpies and activation entropies to the experimental data reported by Agreda and Field for the neutral disproportionation reaction in dilute sulfuric acid (Table 1). The value ΔH_{act}(SMD) = +2.0 kcal/mol is about 3.5 kcal/mol lower than $E^{‡}$ = 5.5 ± 0.1 kcal/mol and ΔS_{act}(SMD) = −39.0 cal K^{-1} mol^{-1} is ≈10.6 cal K^{-1} mol^{-1} more negative than $S^{‡}$ = −28.4 ± 0.2 cal K^{-1} mol^{-1}. This agreement is encouraging, and it is certainly good enough to support our mechanistic proposal for the disproportionation of bromous acid.

CONCLUSION

The thermochemistry was studied of the disproportionation reaction 2HOBrO ⇄ HOBr + $HOBrO_2$ (R4′) and discussed in comparison to reaction R4 of the FKN mechanism of the BZ reaction 2HOBrO ⇄ HOBr + H^+ + BrO_3^-. There has been general agreement that hypobromous acid **1** (pK_a(HOBr) = 8.59) and bromous acid **2** (pK_a(HOBrO) = 3.43) are not dissociated at the typical *pH* value of the BZR. On the other hand, it has generally been assumed that bromic acid **3** is dissociated in typical BZ reactions and that the acid dissociation of bromic acid is responsible for the extra free enthalpy of reaction R4 as compared to reaction R4′. Considering the experimental estimates of $pK_a(\mathbf{3})$ = 0 ± 1.5, it is clear that $\Delta G_a(\mathbf{3})$ is small in magnitude and not nearly large enough to account for the difference between ΔG_4 = −15.7 kcal/mol[25] and $\Delta G_4'$ = −26.0 kcal/mol. Therefore, we conclude that the true ΔG_4 value is close to the computed free enthalpy $\Delta G_4'$= −26.0 kcal/mol for bromous acid disproportionation, i.e., $\Delta G_4 \approx \Delta G_4'$ (Table 4). This conclusion is corroborated by the very good agreement between the computed value $\Delta H_4'$ = −26.1 kcal/mol and the measured value ΔH_4 = -27.2_3 kcal/mol.[28]

The free enthalpies of the reactions HBr + HOBrO ⇄ 2HOBr (R2″) and HBr + $HBrO_3$ ⇄ HOBr + HOBrO (R3″), respectively, were computed, and the best estimates are $\Delta G_2''$(SMD) = -40.2_6 kcal/mol and $\Delta G_3''$(SMD) = -14.2_2 kcal/mol, respectively. Reactions R2″ and R3″ are related to reactions R2 and R3′ via the acidity of aqueous hydrobromic acid, and there remains considerable uncertainty about the value of pK_a(HBr).

Direct O-transfer does not play a significant role in the disproportionation of bromous acid. The discussion of all possible dimeric aggregates **4** of bromous acid, $(HOBrO)_2$, and of the possible mixed aggregates **5**, $(HOBr)(HOBrO_2)$, guided the search for transition states structures **6** for direct O-transfer and four such transition state structures were located. Direct O-transfer is more likely in the 6-membered ring aggregates (**4e** → [**6e**]‡ → **5d** and **4f** → [**6f**]‡ → **5c**) than in the 4-membered ring aggregates (**4b** → [**6b**]‡ → **5a** and **4c** → [**6c**]‡ → **5a**), but the activation processes for all of these processes are too high.

The results of the potential energy surface analysis show that the rate-limiting step in the disproportionation of HOBrO consists of the formation of the hydrate **12a** of anhydride **7**, $O(BrO)_2$, via transition state structure **14a**. The computed activation free enthalpy ΔG_{act}(SMD) = 13.6 kcal/mol for the process 2·**2a** → [**14a**]‡ → **12** corresponds to the reaction rate constant k_4 = 667.5 M^{-1} s^{-1}, and, with the inclusion of error bars of ±1 or ±2 kcal/mol on ΔG_{act}, the computed range for k_4 is in full agreement with the experimental studies by Sullivan and Thompson,[22] Noszticzius et al.,[23] Ariese and Nagy-Ungvarai,[24] Field and Försterling,[25] and the most recent study by Agreda and Field.[28]

The potential energy surface analysis further shows that anhydride **7** is kinetically and thermodynamically unstable with regard to hydrolysis to HOBr and $HOBrO_2$. Anhydride **7** is formed by condensation of two HOBrO molecules via transition state structure **14a** and as a "symmetrical anhydride". However, **7** also is the "mixed anhydride" of HOBr and $HOBrO_2$, and the hydrolysis of **7** to HOBr and $HOBrO_2$ via transition state structure **14b** is exergonic and hardly hindered. At the SMD level, the activation energies for the processes **12a** → [**14b**]‡ and **7a** + H_2O → [**14b**]‡ are ΔG_{298} = 3.7 and ΔG_{298} = 9.0 kcal/mol, respectively. The transition state structure **14b** is much more stable than **14a**, and, hence, the formation of the "symmetrical anhydride" from bromous acid becomes an irreversible reaction for all practical purposes

dx.doi.org/10.1021/jp301329g | J. Phys. Chem. A XXXX, XXX, XXX−XXX

because **7** will instead be hydrolyzed as a "mixed anhydride" to afford HOBr and $HOBrO_2$.

It was shown that the mixed anhydride **8**, $BrO-BrO_2$, does not play a significant role in bromous acid disproportionation. The formation of **8** by the isomerization reaction **7** → **8** is exergonic and kinetically possible, and this isomerization might compete to a small degree with the hydrolysis of **12a** → $[\mathbf{14b}]^{\ddagger}$ → HOBr and $HOBrO_2$. The hydrolysis of hydrate **13** of anhydride **8** to HOBr and $HOBrO_2$ via transition state structure **15** is kinetically hindered with an activation barrier larger than 30 kcal/mol.

Oxygen-transfer between two HOBrO molecules requires nucleophilic attack by a bromine-bound oxygen on bromine. The high lone pair count at the bromine target presents a major obstacle to this nucleophilic attack because lone pair density resists the approach of nucleophiles. The fact that bromous acid is absolutely stable in dilute alkaline solution shows that the neutral disproportionation is shutdown because of the scarcity of HOBrO ($pK_a \approx 3.4$), that any nucleophilic attack on BrO_2^- by either HOBrO or BrO_2^- cannot happen, and, importantly, that any type of nucleophilic attack on HOBrO by BrO_2^- also is impossible. The anhydride mechanism facilitates the O-on-Br attack because a *nucleophilic addition to bromine* is replaced by a *nucleophilic substitution at bromine*. Proton-catalysis most likely will affect the mechanism of disproportionation by provision of the better electrophile $[H_2BrO_2]^+$ as the target of the nucleophilic attack. One can easily envision a proton-assisted variation of the anhydride mechanism involving $[Br(OH)_2]^+$ as OH donor. It is nontrivial to estimate the effects of this type of proton-assistance on the activation barrier because protonation would facilitate the nucleophilic attack on $[Br(OH)_2]^+$, but it might also slow the Br−OH cleavage associated with condensation. On the other hand, proton-catalysis might provide access to one of the paths for direct O-transfer by making the nucleophilic addition of OBrOH to $[Br(OH)_2]^+$ so much better that the substitution at bromine is no longer needed. In this scenario, the electrophile $[(HO)_2Br]^+$ would react with OBrOH and produce protonated bromic acid $[(HO)_2BrO]^+$ and BrOH, and this overall reaction a priori may proceed in one step or in two steps via the intermediate $[(HO)_2Br-O-BrOH]^+$. In a third group of possible mechanisms, one would have to consider reaction paths that involve nucleophilic attack of HOBrO on OH-protonated species $[OBrOH_2]^+$. These paths may proceed with water condensation and formation of $[HOBr-O-BrO]^+$ intermediates or they may lead to HOBr and protonated bromic acid $[O_2BrOH_2]^+$ either directly or via the intermediate $[HOBr-O-BrO(OH_2)]^+$. As can be seen, there is a plethora of options for the proton-catalyzed bromous acid disproportionation, and we plan to explore these options with due diligence in the future.

■ ASSOCIATED CONTENT

Ⓢ Supporting Information

Tables of total energies and thermodynamic data computed at MP2(full)/6-311G* and SMD(MP2(full)/6-311G*) levels, details of rotational energy profiles, and Cartesian coordinates of stationary structures. This material is available free of charge via the Internet at http://pubs.acs.org.

■ AUTHOR INFORMATION

Corresponding Author

*E-mail: glaserr@missouri.edu.

Notes

The authors declare no competing financial interest.

■ ACKNOWLEDGMENTS

This research was supported by NSF-PRISM grant *Mathematics and Life Sciences* (#0928053). The ab initio computations were performed with the HPC resources of the University of Missouri Bioinformatics Consortium (UMBC). We thank Reviewer 1 for his/her careful, insightful, and constructive review.

■ REFERENCES

(1) Belousov, B. P. In *Collections of Abstracts on Radiation Medicine*; Medgiz: Moscow, 1958; p 145.
(2) Zhabotinsky, A. M.; Zaikin, A. N. *Nature* **1970**, *225*, 535−537.
(3) (a) Zhabotinskii, A. M. The early period of systematic studies of oscillations and waves in chemical systems. In *Oscillations Traveling Waves Chem. Syst.*; Field, R. J., Burger, M., Eds.; 1985; pp 1−6. (b) Belousov, B. P. A periodic reaction and its mechanism. In *Oscillations Traveling Waves Chem. Syst.*; Field, R. J., Burger, M., Eds.; 1985; pp 605-660.
(4) Epstein, I. R.; Kustin, K.; De Kepper, P.; Orban, M. *Sci. Am.* **1983**, *248*,112−118, 120, 122−123, 146.
(5) Sobel, S. G.; Hastings, H. M.; Field, R. J. *J. Phys. Chem. A* **2006**, *110*, 5−7.
(6) Keusch, P. Organic Chemistry Demonstration Experiments on Video Chemistry Visualized. University Regensburg, Germany. Online: http://www.demochem.de/D-Video-e.htm [accessed January 1, 2011].
(7) (a) Delgado, J.; Zhang, Ye; Xu, B.; Epstein, I. R. *J. Phys. Chem. A* **2011**, *115*, 2208−2215. (b) Toth, R.; Taylor, A. F. *Prog. React. Kinet. Mech.* **2006**, *31*, 59−115.
(8) (a) Li, H. *Ind. J. Chem. A* **1997**, *36*, 823−828. (b) Lin, H.-P.; Jwo, J.-J. *J. Phys. Chem.* **1995**, *99*, 6897−6902. (c) Doona, C. J.; Kustin, K.; Orban, M.; Epstein, I. R. *J. Am. Chem. Soc.* **1991**, *113*, 7484−7489.
(9) An Introduction to Nonlinear Chemical Dynamics: Oscillations, Waves, Patterns, and Chaos; Epstein, I. R., Pojman, J. A., Eds.; Oxford University Press: New York, NY, 1998. (b) Gray, P.; Scott, S. K. Chemical Oscillations and Instabilities: Non-Linear Chemical Kinetics; Oxford University Press: New York, NY, 1994. (c) Chaos in Chemistry and Biochemistry; Field, R. J., Gyorgyi, L., Eds.; World Scientific Pub. Co.: Hackensack, NJ, 1993.
(10) Muntean, N.; Szabo, G.; Wittmann, M.; Lawson, T.; Fulop, J.; Noszticzius, Z.; Onel, L. *J. Phys. Chem. A* **2009**, *113*, 9102−9108.
(11) Onel, L.; Wittmann, M.; Pelle, K.; Noszticzius, Z.; Sciascia, L. *J. Phys. Chem. A* **2007**, *111*, 7805−7812.
(12) Kurin-Csoergei, K.; Epstein, I. R.; Orban, M. *Nature* **2005**, *433*, 139−142.
(13) Brandl, H. *Prax. Naturwiss., Chem. Sch.* **2008**, *57*, 29−31.
(14) Kolokolnikov, T.; Tlidi, M. *Phys. Rev. Lett.* **2007**, *98*, 188303/1−188303/4.
(15) (a) Yoshida, R. *Adv. Mater.* **2010**, *22*, 3463−3483. (b) Hara, Y.; Maeda, S.; Hashimoto, S.; Yoshida, R. *Intl. J. Mol. Sci.* **2010**, *11*, 704−718. (c) Yashin, V. V.; Kuksenok, O.; Balazs, A. C. *Prog. Polym. Sci.* **2010**, *35*, 155−173.
(16) (a) Field, R. J.; Körös, E.; Noyes, R. M. *J. Am. Chem. Soc.* **1972**, *94*, 8649−8664. (b) Noyes, R. M.; Field, R. J.; Körös, E. *J. Am. Chem. Soc.* **1972**, *94*, 1394−1395.
(17) (a) Tyson, J. J. *Ann. N.Y. Acad. Sci.* **1979**, *316*, 279−295. (b) Tyson, J. J. *J. Phys. Chem.* **1982**, *86*, 3006−3012.
(18) (a) Johnson, B. R.; Scott, S. K.; Thompson, B. W. *CHAOS* **1997**, *7*, 350−358. (b) Györgyi, L.; Field, R. J. *Nature* **1992**, *355*, 808−810. (c) Györgyi, L.; Field, R. J. *J. Phys. Chem.* **1991**, *95*, 6594−6602.
(19) Hegedus, L.; Wittmann, M.; Noszticzius, Z.; Yan, S.; Sirimungkala, A.; Försterling, H.-D.; Field, R. J. *Faraday Discuss.* **2001**, *129*, 21−38.
(20) We write $H_2BrO_2^+$ without any implication regarding the constitution of protonated bromous acid.

(21) Försterling, H. D.; Lamberz, H. J.; Schreiber, H. *Z. Naturforsch., A: Phys., Phys. Chem., Kosmophys.* **1983**, *38A*, 483−486.
(22) Sullivan, J. C.; Thompson, R. C. *Inorg. Chem.* **1979**, *18*, 2375−2379.
(23) Noszticzius, Z.; Noszticzius, E.; Schelly, Z. A. *J. Phys. Chem.* **1983**, *87*, 510−524.
(24) Ariese, F.; Nagy-Ungvarai, Z. *J. Phys. Chem.* **1986**, *90*, 1−4.
(25) Field, R. J.; Försterling, H.-D. *J. Phys. Chem.* **1986**, *90*, 5400−5407.
(26) Försterling, H.-D.; Varga, M. *J. Phys. Chem.* **1993**, *97*, 7932−7938.
(27) Faria, R. d. B.; Epstein, I. R.; Kustin, K. *J. Phys. Chem.* **1994**, *98*, 1363−1367.
(28) Agreda, B. J. A.; Field, R. J. *J. Phys. Chem.* **2006**, *110*, 7867−7873.
(29) Note that $\Delta H_4 = -114$ kJ/mol and $\Delta G_4 = -64$ kJ/mol gives $\Delta S_4 = 167.7$ J/(K mol), or 40.1 cal/(K mol), rather than $\Delta S_4 = -171$ J/(K mol), or −40.9 cal/(K mol), reported in Table 3 of Agreda and Field.
(30) Cramer, C. J. *Essentials of Computational Chemistry*; Wiley: New York, NY, 2004.
(31) Pople, J. A. *Rev. Modern Phys.* **1999**, *71*, 1267−1274.
(32) Wilson, S. *Handb. Mol. Phys. Quantum Chem.* **2003**, *2*, 314−373.
(33) (a) Krishnan, R.; Binkley, J. S.; Seeger, R.; Pople, J. A. *J. Chem. Phys.* **1980**, *72*, 650−654. (b) Curtiss, L. A.; Binning, R. C., Jr. *Intl. J. Quantum Chem.* **1991**, *40*, 781−787.
(34) Frisch, M. J., Trucks, G. W., Schlegel, H. B., Scuseria, G. E., Robb, M. A., Cheeseman, J. R., Scalmani, G., Barone, V., Mennucci, B., Petersson, G. A. et al. *Gaussian 09, Rev. A.1*; Gaussian, Inc.: Wallingford, CT, 2009.
(35) Dennington, R.; Keith, T.; Millam, J. *GaussView* 5.0.8; Semichem Inc.: Shawnee Mission, KS, 2009.
(36) (a) Wahlin, P.; Schimmelpfennig, B.; Wahlgren, U.; Grenthe, I.; Vallet, V. *Theor. Chem. Acc.* **2009**, *124*, 377−384. (b) Kongsted, J.; Mennucci, B. *J. Phys. Chem. A* **2007**, *111*, 9890−9900. (c) Jensen, L.; van Duijnen, P. Th. The Discrete Solvent Reaction Field Model: A Quantum Mechanics/Molecular Mechanics Model for Calculating Nonlinear Optical Properties of Molecules in Condensed Phase. In *Atoms, Molecules and Clusters in Electric Fields. Theoretical Approaches to the Calculation of Electric Polarizability*, 1st ed.; Maroulis, G., Ed.; Imperial College Press: London, 2006; pp 283−325.
(37) (a) Ribeiro, R. F.; Marenich, A. V.; Cramer, C. J.; Truhlar, D. G. *J. Comput.-Aided Mater.* **2010**, *24*, 317−333. (b) Marenich, A. V.; Cramer, C. J.; Truhlar, D. G. *J. Phys. Chem. B* **2009**, *113*, 6378−6396.
(38) (a) Marenich, A. V.; Cramer, C. J.; Truhlar, D. G. *J. Phys. Chem. B* **2009**, *113*, 4538−4543. (b) Halim, M. A.; Shaw, D. M.; Poirier, R. A. *THEOCHEM* **2010**, *960*, 63−72. (c) Saielli, G. *J. Phys. Chem. A* **2010**, *114*, 7261−7265.
(39) Cancès, E.; Mennucci, B.; Tomasi, J. *J. Chem. Phys.* **1997**, *107*, 3032−3041.
(40) (a) Tomasi, J.; Cappelli, C.; Mennucci, B.; Cammi, R. From Molecular Electrostatic Potentials to Solvation Models and Ending with Biomolecular Photophysical Processes. In *Quantum Biochemistry*, 1st ed.; Matta, C. F., Ed.; Wiley-VCH: Weinheim, Germany, 2010; pp 131−170. (b) Tomasi, J. Modern Theories of Continuum Models: The Physical Model. In Continuum Solvation Models in Chemical Physics: From Theory to Application, 1st ed.; Mennucci, B., Cammi, R., Eds.; John Wiley & Sons Ltd.: West Sussex, 2007; pp 1−28.
(41) Experimental Studies of HOBr: (a) Ruscic, B.; Berkowitz, J. *J. Chem. Phys.* **1994**, *101*, 7795−7803. (b) Qiao, Z.; Sun, S.; Sun, Q.; Zhao, J.; Wang, D. *J. Chem. Phys.* **2003**, *119*, 7111−7114.
(42) Theoretical Studies of HOBr: (a) Peterson, K. A. *J. Chem. Phys.* **2000**, *113*, 4598−4612. (b) Azzam, T.; Schinke, R.; Farantos, S. C.; Joyeux, M.; Peterson, K. A. *J. Chem. Phys.* **2003**, *116*, 9643−9652. (c) Balint-Kurti, G. G.; Fusti-Molnar, L.; Brown, A. *Phys. Chem. Chem. Phys.* **2001**, *3*, 702−710. (d) Santos, C. M. P.; Faria, R. B.; De Almeida, W. B.; Machuca-Herrera, J. O.; Machado, S. P. *Can. J. Chem.* **2003**, *81*, 961−970. (e) Santos, C. M. P.; Faria, R.; Machado, S. P.; De Almeida, W. B. *J. Chem. Phys.* **2004**, *121*, 141−148. (f) Solimannejad, M.; Alkorta, I.; Elguero, J. *Chem. Phys. Lett.* **2008**, *454*, 201−206.
(43) Experimental Studies of $HBrO_2$: Akai, N.; Wakamatsu, D.; Yoshinobu, T.; Kawai, A.; Shibuya, K. *Chem. Phys. Lett.* **2010**, *499*, 117−120.
(44) Theoretical Studies of $HBrO_2$: (a) Sumathi, R.; Peyerimhoff, S. D. *Phys. Chem. Chem. Phys.* **1999**, *1*, 3973−3979. (b) Lee, T. J. *Chem. Phys. Lett.* **1996**, *262*, 559−566.
(45) Theoretical Studies of $HBrO_3$: Guha, S.; Francisco, J. S. *J. Phys. Chem. A* **1998**, *102*, 2072−2079.
(46) Santos, C. M. P.; Faria, R. B.; Machuca-Herrera, J. O.; Machado, S.; De, P. *Can. J. Chem.* **2001**, *79*, 1135−1144.
(47) (a) Nagy, P.; Ashby, M. T. *J. Am. Chem. Soc.* **2007**, *129*, 14082−14091. (b) See Table 1 in the following : Swain, P. A. *Educ. Chem.* **1983**, 219−221.
(48) Faria, R. d. B.; Epstein, I. R.; Kustin, K. *J. Phys. Chem.* **1992**, *96*, 6861−6863.
(49) (a) Eyet, N.; Villano, S. M.; Bierbaum, V. M. *Int. J. Mass Spectrom.* **2009**, *283*, 26−29. (b) Blanksby, S. J.; Ramond, T. R.; Davico, G. E.; Nimlos, M. R.; Kato, S.; Bierbaum, V. M.; Lineberger, W. C.; Ellison, G. B.; Okumura, M. *J. Am. Chem. Soc.* **2001**, *123*, 9585−9596.
(50) Bhattacharyya, R.; Lahiri, S. C. *Z. Phys. Chem.* **2010**, *224*, 1389−1410.
(51) Maurer, P.; Iftimie, R. *J. Chem. Phys.* **2010**, *132*, 074112−16.
(52) Kamble, D. L.; Nandibewoor, S. T. *Int. J. Chem. Kinet.* **1996**, *28*, 673−679.
(53) Vauleugenhaghe, C.; Valensi, G.; Pourbaix, M. In *Atlas of Electrochemical Equilibrium in Aqueous Solutions*, 2nd ed.; Pourbaix, M., Ed.; National Association of Corrosion Engineers: Houston, 1974; p 604.
(54) Reddy, C. S.; Sundaram, E. V. *Indian J. Chem.* **1987**, *26A*, 118−123.
(55) Côrtes, C. E. S.; Faria, R. B. *J. Braz. Chem. Soc.* **2001**, *12*, 775−779.
(56) Petkovic, P. M. *J. Chem. Soc., Dalton Trans.* **1982**, 2425−2427.
(57) Knopf, D. A.; Luo, B. P.; Krieger, U. K.; Koop, T. *J. Phys. Chem. A* **2003**, *107*, 4322−4332.
(58) Marcus, Y. *J. Chem. Soc., Faraday Trans. 1* **1979**, *75*, 1715−1727.
(59) (a) d(Br−OH) in Å in chair-**4a**: 1.80; boat-**4a**: 1.80; **4b**: 1.86, 1.88; **4c**: 1.95, 1.86; cis-**4d**: 1.93; trans-**4d**: 1.93; **4e**: 1.85, 1.82; **4f**: 1.97, 1.83 Å; **4g**: 1.83, 1.89. (b) d(Br−O) in Å in chair-**4a**: 1.68; boat-**4a**: 1.68; **4b**: 1.66, 1.66; **4c**: 1.67, 1.65; cis-**4d**: 1.64; trans-**4d**: 1.64; **4e**: 1.67, 1.68; **4f**: 1.64, 1.66 Å; **4g**: 1.67, 1.64.
(60) The BrO_2 planes are close to perpendicular in T-contact aggregates in analogy to common nomenclature of arene-arene contacts.
(61) Buxton, G. V.; Dainton, F. S. *Proc. R. Soc. London, Ser. A* **1968**, *304*, 427−439.
(62) Guha, S.; Francisco, J. S. *Chem. Phys. Lett.* **2001**, *346*, 497−502.
(63) (a) Olson, L. P.; Kuwata, K. T.; Bartberger, M. D.; Houk, K. N. *J. Am. Chem. Soc.* **2002**, *124*, 9469−9475. (b) Roth, W. R.; Bastigkeit, T.; Boerner, S. *Liebigs Ann.n* **1996**, 1323−1328. (c) Olson, J. B.; Koch, T. H. *J. Am. Chem. Soc.* **1986**, *108*, 756−761. (d) Menon, A.; Sathyamurthy, N. *J. Phys. Chem.* **1981**, *85*, 1021−1023.
(64) Chemical Kinetics and Reaction Dynamics; Dover Publications: Mineola, NY, 2006. (b) House, J. E. Principles of Chemical Kinetics, 2/e; Academic Press: Waltham, MA, 2007.

dx.doi.org/10.1021/jp301329g | *J. Phys. Chem. A* XXXX, XXX, XXX−XXX